

AN ELASTIC-PLASTIC FRACTURE CRITERION  
BASED ON THE CONCEPT OF STRAIN  
TOLERANCE

by

Conrad F. Fiftal

ARTHUR LAKES LIBRARY  
COLORADO SCHOOL OF MINES  
GOLDEN, COLORADO

8426/100  
OH

ProQuest Number: 10796065

All rights reserved

INFORMATION TO ALL USERS

The quality of this reproduction is dependent upon the quality of the copy submitted.

In the unlikely event that the author did not send a complete manuscript and there are missing pages, these will be noted. Also, if material had to be removed, a note will indicate the deletion.



ProQuest 10796065

Published by ProQuest LLC (2019). Copyright of the Dissertation is held by the Author.

All rights reserved.

This work is protected against unauthorized copying under Title 17, United States Code  
Microform Edition © ProQuest LLC.

ProQuest LLC.  
789 East Eisenhower Parkway  
P.O. Box 1346  
Ann Arbor, MI 48106 – 1346

A Thesis submitted to the Faculty and the Board of Trustees of the Colorado School of Mines in partial fulfillment of the requirements for the degree of Doctor of Philosophy in Metallurgical Engineering.

Signed: Conrad F. Fiftal  
Conrad F. Fiftal

Golden, Colorado

Date: April 30, 1974

Approved: W. L. Bradley  
Walter L. Bradley  
Thesis Advisor

John P. Hager  
John P. Hager  
Head of Department

Golden, Colorado

Date: 4/30, 1974

ARTHUR LAKES LIBRARY  
COLORADO SCHOOL OF MINES  
GOLDEN, COLORADO

ABSTRACTARTHUR LAKES LIBRARY  
COLORADO SCHOOL OF MINES  
GOLDEN, COLORADO

A semiempirical elastic-plastic fracture criterion has been developed for predicting defect-controlled failure when gross plastic deformation is involved. This new criterion utilizes the strain tolerance of the material in the presence of a defect as the engineering performance parameter. Strain tolerance, defined as the nominal total strain at failure, is related to defect size and is shown to be an extension of linear elastic fracture mechanics in the tough region.

Strain tolerance data are presented for 2014-T6 aluminum, 6Al-4V titanium-STA, and A533B steel containing semielliptical surface flaws. The effect of flaw geometry and specimen restraint on strain tolerance is also shown. The interaction effects between surface flaws and plastic strain gradients due to holes are presented, and comparison is made with analytical elastic predictions from linear elastic fracture mechanics.

An application-of-principle example is presented to show safety factor calculations for a pressure vessel containing a surface flaw at a plastic strain concentration such as a nozzle opening.

TABLE OF CONTENTS

	Page
LIST OF FIGURES. . . . .	vi
LIST OF TABLES . . . . .	viii
ACKNOWLEDGMENTS. . . . .	ix
INTRODUCTION . . . . .	1
EXPERIMENTAL PROCEDURE . . . . .	9
Nominal Material Property Data. . . . .	9
Specimen Design . . . . .	11
Surface Flaw Introduction . . . . .	19
Strain Tolerance Measurement. . . . .	20
RESULTS AND ANALYSIS . . . . .	26
Baseline Strain Tolerance . . . . .	26
Material Variation Effect . . . . .	32
Thickness Restraint Effect. . . . .	36
Flaw Geometry Effect. . . . .	41
Strain Gradient Effect. . . . .	41
Circular Hole Geometry Tests . . . . .	44
Circular Hole-Edge Crack Geometry Tests. . . . .	56
CONCLUSIONS. . . . .	68
DESIGN APPLICATION OF THE STRAIN TOLERANCE FRACTURE CRITERION . . . . .	71

	Page
RECOMMENDATIONS FOR FUTURE WORK. . . . .	75
APPENDICES:	
A. Strain Tolerance Data for 2014-T6 Aluminum (Heat 6670), 6Al-4V Titanium-STA, and A533B Steel . . . . .	76
B. Elastic Strain Tolerance Calculations from Linear Elastic Fracture Mechanics . . . . .	84
C. Calculation of a Semiempirical Equation for Strain Tolerance in the Elastic-Plastic Region. . . . .	89
D. Neuber Approximation of the Plastic Strain Concentration Factor for a Notch. . . . .	96
E. Elastic Strain Gradient Effect for a Circular Hole-Edge Crack Geometry from Linear Elastic Fracture-Mechanics . . . . .	100
LITERATURE CITED . . . . .	109

ARTHUR LAKES LIBRARY  
COLORADO SCHOOL OF MINES  
GOLDEN, COLORADO

LIST OF FIGURES

ARTHUR LAKES LIBRARY  
 COLORADO SCHOOL OF MINES  
 GOLDEN, COLORADO

Figure	Page
1. Strain Tolerance Specimen for 2014-T6 Aluminum . . . . .	14
2. Strain Tolerance Specimen for 6Al-4V Titanium-STA . . . . .	15
3. Strain Tolerance Specimen for A533B Steel. . . . .	16
4. Modification of the 2014-T6 Aluminum Strain Tolerance Specimen for Determination of the Effect of Thickness Restraint, Edge Crack Geometry, and Strain Gradient Due to a Hole. . . . .	18
5. EDM Tool Shape for Center Crack, Edge Crack, and Circular Hole-Edge Crack Geometries. . . . .	21
6. Strain Tolerance Curve for 2014-T6 Aluminum (Heat 6670) at Room Temperature. . . . .	27
7. Strain Tolerance Curve for 6Al-4V Titanium-STA at Room Temperature. . . . .	28
8. Strain Tolerance Curves for A533B Steel (HSST Plate 01) at -20°F and 5°F . . . . .	29
9. Elastic Strain Concentration Gradients for Holes in Finite Width Plate, Based on Nominal Strain . . . . .	47
10. Peak and Nominal Strain as a Function of Net Section Stress for a 0.750-Inch-Diameter Hole . . . . .	48
11. Peak and Nominal Strain as a Function of Net Section Stress for a 0.500-Inch-Diameter Hole. . . . .	49
12. Peak and Nominal Strain as a Function of Net Section Stress for a 0.250-Inch-Diameter Hole. . . . .	50

Figure	Page
13. Peak and Nominal Strain as a Function of Net Section Stress for a 0.126-Inch-Diameter Hole. .	51
14. Peak Strain Concentration Factor, For a Circular Hole in 2014-T6 Aluminum, as a Function of Net Section Stress or Strain . . . .	53
15. Elastic Strain Gradient Effect for a Circular Hole-Edge Crack Geometry . . . . .	58
16. Plastic Strain Gradient Effect in 2014-T6 Aluminum for a Circular Hole-Edge Crack Geometry in a Fully Plastic Net Section. . . . .	63
17. Plastic Strain Concentration Gradients at Fracture in 2014-T6 Aluminum for a Circular Hole-Edge Crack Geometry . . . . .	66
C-1. Stress-Strain Curve for 2014-T6 Aluminum . . . .	92
C-2. Stress-Strain Curve for 6Al-4V Titanium-STA. . .	93
C-3. Stress-Strain Curve for A533B Steel. . . . .	94
E-1. Circular Hole-Edge Crack Geometry in Infinite Plate . . . . .	102
E-2. Stress Function $F(a/R)$ for Circular Hole-Edge Crack Geometry. . . . .	104
E-3. Elastic Strain Gradient Effect for a Circular Hole-Edge Crack Geometry. . . . .	105

LIST OF TABLES

Table	Page
1. Comparison of the Design Approach of Linear Elastic Fracture Mechanics With That of Strain Tolerance . . . . .	7
2. Chemical Analysis for 2014-T6 Aluminum, 6Al-4V Titanium-STA, and A533B Steel . . . . .	10
3. Semiempirical Equation for Strain Tolerance as a Function of Crack Size for 2014-T6 Aluminum (Heat 6670), 6Al-4V Titanium-STA, and A533B Steel. . . . .	33
4. Strain Tolerance Data for 2014-T6 Aluminum (Heat 5867) at Room Temperature. . . . .	34
5. Thickness Restraint Effect on Strain Tolerance of 2014-T6 Aluminum (Heat 6670). . . . .	38
6. Edge-Crack Flaw Geometry Effect on Strain Tolerance of 2014-T6 Aluminum (Heat 6670). . . . .	42
7. Peak Elastic Strain Concentration Factors for Holes in Finite Width Plate, Based on Net Section Strain . . . . .	45
8. Strain Gradient Effect on Strain Tolerance of 2014-T6 Aluminum (Heat 6670). . . . .	60
A-1. Strain Tolerance Data for 2014-T6 Aluminum (Heat 6670) at Room Temperature. . . . .	78
A-2. Strain Tolerance Data for 6Al-4V Titanium-STA at Room Temperature. . . . .	80
A-3. Strain Tolerance Data for A533B Steel at -20°F . . . . .	82
B-1. Fracture Toughness Data for 2014-T6 Aluminum, 6Al-4V Titanium-STA, and A533B Steel . . . . .	86

ACKNOWLEDGMENTS

The author wishes to sincerely thank Dr. J. D. Lubahn, Professor of Basic Engineering, for his technical advice and general encouragement during the course of this study.

Particular appreciation is extended to Dr. W. L. Bradley, Professor of Metallurgical Engineering, for his counsel during preparation of the final manuscript.

The author wishes to gratefully acknowledge the General Electric Company-Nuclear Energy Division for financial assistance during the initiation of the research program and the Martin Marietta Corporation-Aerospace Division, whose continued financial support and testing facilities made the completion of this study possible.

Special appreciation goes to the author's wife, Jean, for her patience, understanding, and faith over the long road.

INTRODUCTION

The objective of this research is to develop an elastic-plastic fracture criterion, for predicting defect-controlled failure when gross plastic deformation is involved, that will be an extension of linear elastic fracture mechanics. This new criterion will utilize the strain tolerance of the material in the presence of a defect as the engineering performance parameter. Since the strain tolerance concept is entirely new and unproven, this research will provide the analytical and experimental development required to define its capabilities and limits in the design of structural hardware. In order to place the strain tolerance fracture criterion in proper perspective a short review of the state-of-the-art of fracture mechanics will be helpful.

Sudden bursting or collapsing of welded structures may occur at nominal stresses below the yield strength if a combination of unfavorable material and stress conditions exist at the location of inadvertent flaws. Such failure that occurs suddenly and without warning, that propagates rapidly to a point where structural integrity is impaired, and often to the point of complete separation is characterized as "brittle fracture".

Until the advent of linear elastic fracture mechanics about 20 years ago, pressure vessels and similar structures were designed primarily on the basis of yield strength and room-temperature notched-bar impact strength. Several low-temperature failures of welded ships and T-2 tankers<sup>(1)</sup> showed the fallacy of characterizing fracture resistance using room-temperature notch toughness. A material with a high notch toughness at room temperature may have its ductile-to-brittle failure transition occurring at a higher temperature than a material with a lower room-temperature notch toughness. Thus, the original notched-bar impact requirement evolved into the transition temperature method<sup>(2)</sup>. Criteria for determining the transition temperature for a material were based on transition in energy absorbed, change in fracture appearance, or transition in ductility. The concept was implemented by limiting the operating temperature of the structure to values above the transition temperature or by selecting a material whose transition temperature was lower than the operating temperature. Success in preventing failure was achieved by using the transition temperature method, whose main advantage was that the necessary stress analysis for the structure was simple, requiring only avoidance of gross plastic flow. Its overriding disadvantage was that, by not relating flaw size and shape to critical stress levels, it carried many undesirable

penalties, such as prohibiting use of high-strength materials with high transition temperatures, operating structures at undesirably high temperatures to remain in the ductile range, or using expensive materials to achieve a required toughness which placed structural designs at a competitive disadvantage.

Fortunately during the ensuing time, linear elastic fracture mechanics was developed to the point where it has been used reliably to insure structural integrity for thin-walled aerospace pressure vessels fabricated from aluminum, titanium, and steel alloys having high strength-to-density ratios<sup>(3)</sup>. Briefly, the linear elastic fracture mechanics concept involves the practice of preventing brittle fracture by limiting nominal stress to a value compatible with flaw size. The analytical basis for linear elastic fracture mechanics is the elastic analysis of the crack tip region which shows a unique stress field with a singularity at the crack tip that dominates all other geometrical features. The strength of this crack tip singularity is the normal opening mode stress intensity factor,  $K_I$ , which is a function of nominal stress and crack size. Fracture occurs at a critical value of  $K_I$  called the fracture toughness,  $K_{Ic}$ , which is considered to be a material property.

Linear elastic fracture mechanics in its current state of evolvment is limited to cases where small crack-tip plasticity is involved, that is, for low-toughness materials

ARTHUR LAKES LIBRARY  
COLORADO SCHOOL OF MINES  
GOLDEN, COLORADO

at nominal stresses well below the yield strength. However, there are many important design situations where it is desirable to have a failure criterion which could predict defect-controlled failure for cases of both small- and large-scale plasticity. For example, medium-strength steels of high fracture toughness used in heavy-section nuclear-reactor pressure vessels generally exhibit considerable crack-tip plasticity, that limits the applicability of linear elastic fracture mechanics and forces major reliance on the transition temperature method. Also, in many design situations using both high- and medium-strength materials, stress concentrations are an integral part of the structure and typically involve local stresses above the yield strength. A pressure vessel will usually have nozzle openings (holes) with fillet weld attachment of piping. This area is a very common site for surface or buried defects inadvertently formed during fabrication.

A direct extension of linear elastic fracture mechanics concepts to cases of large-scale yielding would assume again the existence of a crack tip singularity. Work by Hutchinson<sup>(4)</sup> and Rice and Rosengren<sup>(5)</sup> shows that a strain singularity does exist which is uniquely dependent upon the material flow properties. Attempts to characterize the crack tip strain singularity have required using numerical nonlinear finite element analysis<sup>(6,7)</sup>. However, in the

region where the most accuracy is desired, the crack tip, finite elements are inherently the least accurate. The characterization of the crack tip area by a parameter whose value depends upon the near tip stress-strain field but whose measurement is remote from the crack tip would provide a more practical method for analyzing fracture. Currently there are two promising approaches to elastic-plastic fracture that avoid the problem of crack-tip modeling: the J-integral concept of Rice<sup>(8)</sup> and the strain tolerance approach of Randall<sup>(9)</sup>. Both approaches consider average deformation occurring over an arbitrary area remote from the crack tip. In the J-integral concept, the engineering performance parameter is the rate of change in deformation energy with respect to crack area at fracture. Similarly, the nominal fracture strain is the critical parameter in the strain tolerance approach.

The potential of the J-integral as a fracture criterion has been advanced by Begley and Landes<sup>(10)</sup>. J can be found experimentally by using a series of identical specimens of thickness, B, with differing crack lengths (a). The area under the load versus load point deflection curves is deformation energy (E). Deformation energy is plotted as a function of crack length for fixed values of deflection ( $\delta$ ). The slopes of the curves ( $\frac{1}{B} \frac{dE}{da}$ ) for given crack lengths, plotted as a function of deflection, is equal to J. The

critical  $J$  at fracture ( $J_c$ ) is found from values of  $\delta$  and  $a$  at the onset of instability. In the elastic range  $J$  is equal to the strain energy release rate ( $G$ ) from linear elastic fracture mechanics. Initial tests on a Ni-Cr-Mo-V steel in the plastic range by Landes and Begley<sup>(11)</sup> show that  $J_c$  may be essentially independent of crack length and geometry, hence a material constant. For application to design of practical hardware, the safety factor would be the ratio of critical  $J$  to applied  $J$ . The calculation of applied  $J$  requires solutions for  $J$  as a function of crack size and applied strain (or applied load) for various component geometries. Until these solutions are developed, ready application of the  $J$ -integral concept is limited.

The potential of strain tolerance as a fracture criterion has been advanced by Lubahn<sup>(12)</sup>. The basic premise is that nominal total strain (elastic plus plastic) at failure, defined as strain tolerance, can be related to defect size. The safety factor against defect controlled failure would be the ratio of material strain tolerance to applied strain in the hardware. A general outline of the fracture analysis required using the strain tolerance concept is illustrated in Table 1. Note that the approach is similar to that of linear elastic fracture mechanics except that strain, rather than stress, is the engineering performance parameter. In fact, at stresses below the yield strength, the strain

TABLE 1. Comparison of the Design Approach of Linear Elastic Fracture Mechanics With That of Strain Tolerance

	<u>Elastic Fracture Mechanics</u>	<u>Strain Tolerance</u>
Applicability:	Elastic	Elastic-Plastic
Performance Parameter:	Stress	Strain
Safety Factor for Fracture:	$\frac{\text{Critical Stress}}{\text{Applied Stress}}$	$\frac{\text{Critical Strain}}{\text{Applied Strain}}$
Critical Parameter Value:	Analytical Stress vs Flaw Size Equation + Experimental Fracture Toughness Constant for Material	Empirical Strain vs Flaw Size Relationship for Material
Applied Parameter Value:	Linear Elastic Stress Analysis for Structure	Non-linear Strain Analysis for Structure

tolerance is identical to the nominal elastic fracture strain predicted from linear elastic fracture mechanics.

In general, material strain tolerance will be a function of flaw size and temperature. It may also be a function of stress state, geometrical restraint, flaw geometry, and strain gradient. Baseline strain tolerance versus flaw size curves will be determined for two high strength-low toughness materials at room temperature: 2014-T6 aluminum and 6Al-4V titanium-STA, and one medium strength-high toughness material at  $-20^{\circ}\text{F}$ : A533B steel. The effect of material variations, thickness restraint, flaw geometry, and strain gradient on the baseline strain tolerance curve for 2014-T6 aluminum will be investigated. An application-of-principle example will also be developed by using the strain tolerance fracture criteria to show safety factor calculations for a 2014-T6 aluminum pressure vessel containing a surface flaw at a plastic strain concentration, such as a nozzle opening.

## EXPERIMENTAL PROCEDURE

The concept of strain tolerance as a basis for an elastic-plastic fracture criterion was introduced, and the experimental program briefly outlined, in the previous section. This section will discuss in detail the nominal properties of the test materials, the design of test specimens, the introduction of surface flaws in the test specimens, and the measurement of strain tolerance.

### Nominal Material Property Data

2014-T6 aluminum and 6Al-4V titanium-STA in the form of wrought plate were chosen for this study because they are typical of low toughness materials used in thin-walled aerospace pressure vessels where high strength-to-density ratios are a necessity for weight savings. 2014-T6 aluminum (60 ksi yield, 35 ksi  $\sqrt{\text{in.}}$  toughness) and 6Al-4V titanium-STA (160 ksi yield, 45 ksi  $\sqrt{\text{in.}}$  toughness) have strength-to-density ratios equal to 600 and 1000 ( $\text{in.} \times 10^3$ ) respectively. Spectrographic chemical analyses for two heats of 2014-T6 aluminum and for 6Al-4V titanium-STA are shown in Table 2.

A533B steel was chosen for this study because it is typical of the high toughness-medium strength materials used



in land based nuclear reactor pressure vessels, where weight savings is not a predominant consideration. A533B steel (65 ksi yield, 180 ksi  $\sqrt{\text{in.}}$  toughness) has a strength-to-density ratio equal to 230 (in.  $\times 10^3$ ). The A533B steel came from the heavy section steel technology program (HSSTP) of the Atomic Energy Commission. All 2-in.-thick stock was cut from a section 2 to 4 inches from the top of 12-in.-thick HSST plate 01. A chemical analysis for this heat of A533B steel is given in Table 2.

#### Specimen Design

The basic laboratory specimen that was used for measurement of material strain tolerance in the presence of a defect was a tensile specimen that contained a central semielliptical surface flaw oriented perpendicular to the applied load. The surface flaw was chosen because it was most representative of natural flaws encountered in practical hardware. The strain tolerance specimen was designed to cover the complete failure range from elastic to fully plastic using the following guidelines:

- (1) The gage section must be large enough to provide sufficient restraint for valid fracture toughness determination in the elastic region with large flaws. Linear elastic fracture mechanics only applies to cases of limited crack tip plasticity. A sufficiently large

ARTHUR LAKES LIBRARY  
COLORADO SCHOOL OF MINES  
GOLDEN, COLORADO

ligament width\* and thickness will decrease the size of the plastic zone at the crack tip by virtue of preventing lateral contraction of material ahead of the crack tip, thereby inducing a state of triaxial tension. The local stress distribution at the tip of a crack is such that the size of the plastic zone will be proportional to the square of the fracture toughness-to-yield strength ratio  $(K_{Ic}/S_y)^2$ (13). Therefore, ligament width and thickness should also be proportional to the ratio  $(K_{Ic}/S_y)^2$ . Experimental results for through-thickness flaws in high strength steel, titanium, and aluminum alloys indicate that dimensions of thickness and ligament width that show full restraint range from a low of  $0.4 (K_{Ic}/S_y)^2$  for 4340 steel (210 ksi yield) to a high of  $3.4 (K_{Ic}/S_y)^2$  for maraged steel (280 ksi yield)(14). A practical, though sometimes conservative estimate has been suggested as  $2.5 (K_{Ic}/S_y)^2$ (15).

- (2) The gage section must be wide enough to measure nominal strain, as opposed to local strain, on the plane of the flaw for valid strain tolerance determination in the plastic region with small flaws. The plastic strain distribution around a semielliptical surface flaw has

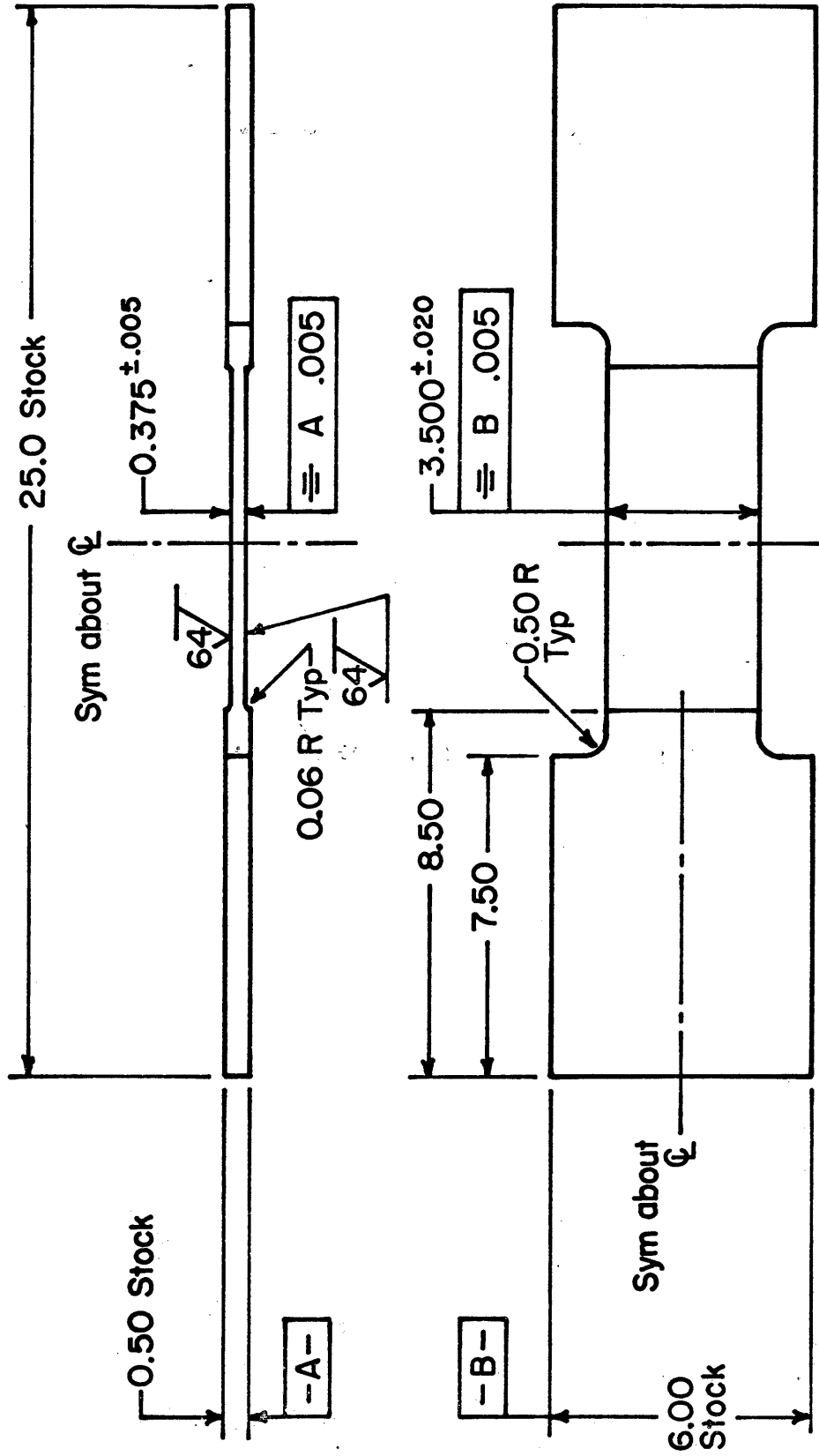
---

\*The ligament width is defined as the distance between the crack tip and the edge of the gage section.

been measured by Beck in 4340 steel<sup>(16)</sup> and in 2014-T6 aluminum<sup>(17)</sup>. The distance away from the crack tip where the local strain is only 10 percent above nominal is equal to three half-crack lengths ( $3c$ ) when the section is elastic, but on the verge of yielding, to ten half-crack lengths ( $10c$ ) when the section is fully plastic. This would indicate that the specimen width required for valid strain tolerance measurement needs to be equal to four crack lengths [ $4(2c)$ ] when the section is elastic and eleven crack lengths [ $11(2c)$ ] when the section is fully plastic.

- (3) Sample design must also have the normal size restraints to minimize material and machining costs and to fail within the available load capacity of the test machine.

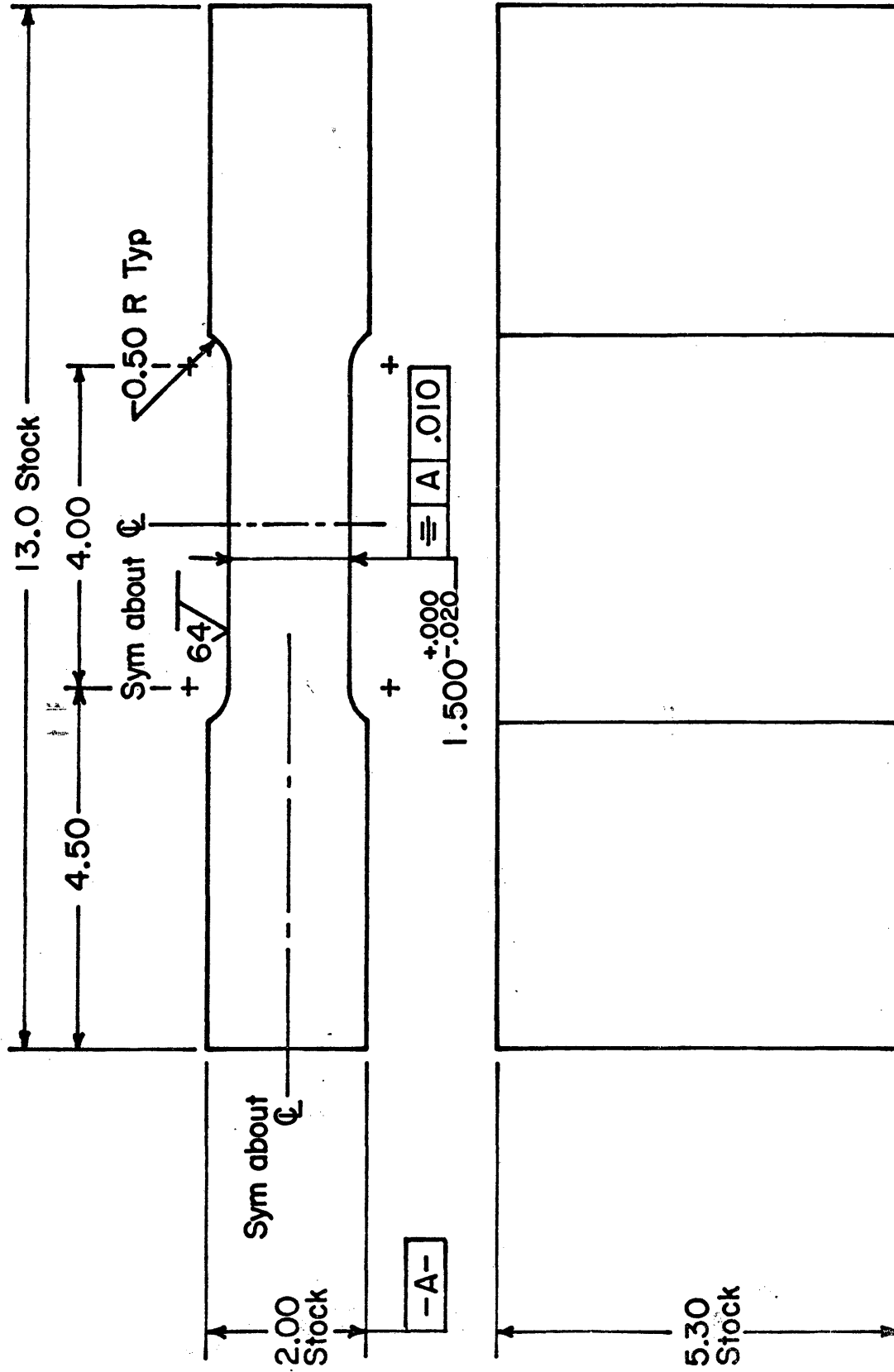
The tensile specimen design for 2014-T6 aluminum, 6Al-4V titanium-STA, and A533B steel is shown in Figures 1, 2, and 3, respectively. The specimen ends were made to be friction gripped using laterally applied hydraulic pressure. Nominal thicknesses conveniently available consisted of 0.50-in.-thick 2014-T6 aluminum plate, 0.090-in.-thick 6Al-4V titanium sheet, and 2-in.-thick A533B steel plate. Flaw depths were never more than half the thickness. The ratio of thickness-to- $(K_{Ic}/S_y)^2$  ranged from 1.1 for titanium to 1.7 for steel. The ratio of ligament width-to- $(K_{Ic}/S_y)^2$  for the largest flaw that caused elastic failure ranged from 2.5 for



**Note: Avoid Undercutting Gage Section at Fillet Tangency Points.**

Figure 1. Strain Tolerance Specimen for 2014-T6 Aluminum.





Note: Avoid Undercutting Gage Section at Fillet Tangency Points.

Figure 3. Strain Tolerance Specimen for A533B Steel.

ARTHUR LAKES LIBRARY  
COLORADO SCHOOL OF MINES  
GOLDEN, COLORADO

steel to 9.4 for titanium. Thus, the specimen gage section had adequate size for a valid fracture toughness determination. The ratio of specimen width-to-flaw length ( $W/2c$ ) for the largest flaw when failure was elastic ranged from 5.1 for steel to 13.5 for titanium, and when failure was plastic ranged from 11.1 for steel to 27.8 for aluminum. Therefore, the specimen gage section also had adequate width for valid strain tolerance measurements. The restraint in the width direction is probably at its maximum and can be considered to be "full width restraint".

The basic 2014-T6 aluminum center-crack strain tolerance specimen given in Figure 1 was modified for determination of the effect of thickness restraint, flaw geometry, and strain gradient. The thickness restraint specimen was identical to the strain tolerance specimen except that thickness was varied. The flaw geometry specimen consisted of two quarter-elliptical surface cracks at the edges of the specimen. The strain gradient specimen contained two quarter-elliptical surface cracks at the edges of a centrally located, through-thickness hole. Specimen width was still sufficient to measure nominal strain at the edge of the specimen. These various specimen geometries are schematically shown in Figure 4.

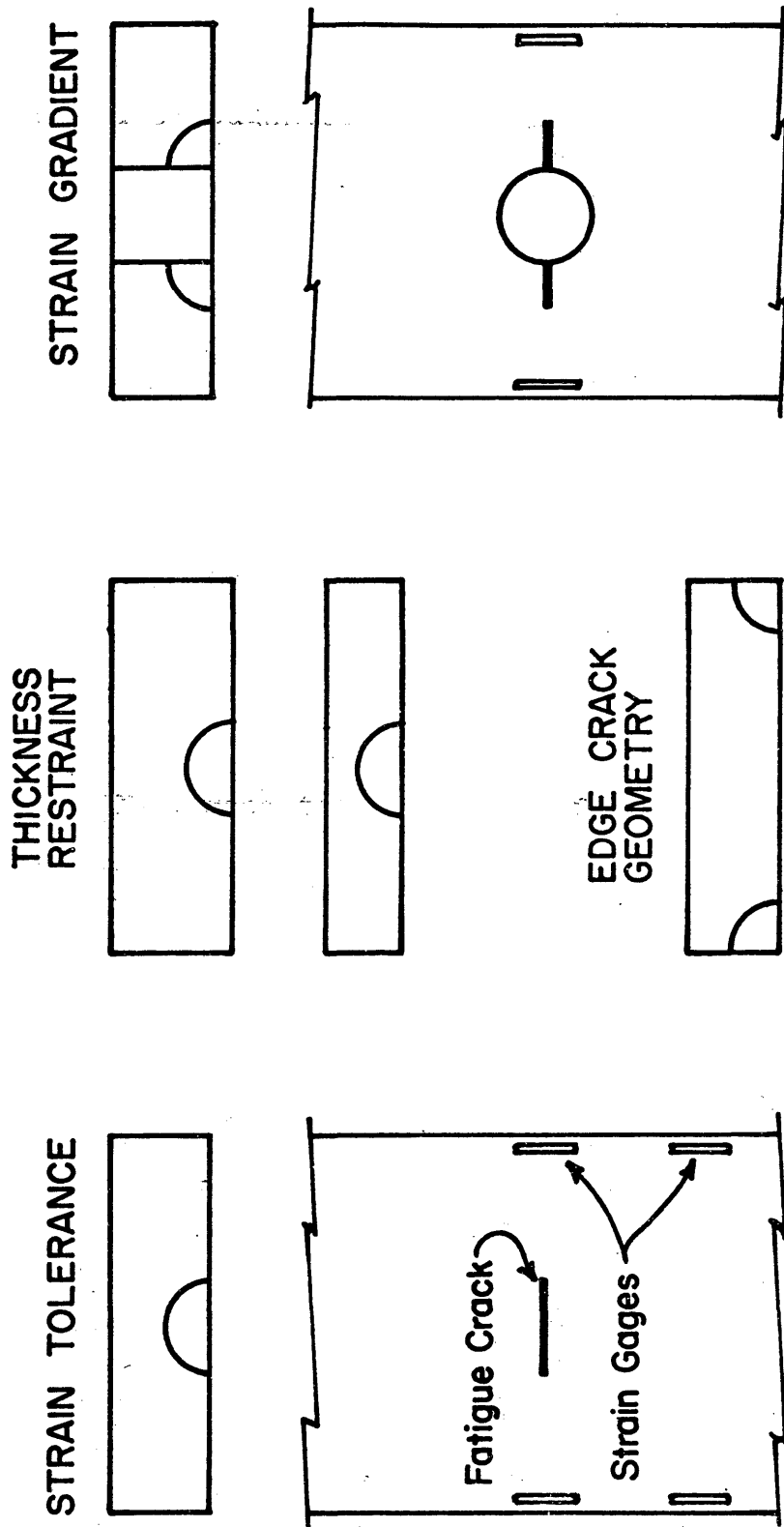


Figure 4. Modification of the 2014-T6 Aluminum Strain Tolerance Specimen for Determination of the Effect of Thickness Restraint, Edge Crack Geometry, and Strain Gradient Due to a Hole.

### Surface Flaw Introduction

After specimen machining, a surface flaw was introduced in the gage section by tension-fatigue extension of an electric-discharge machined (EDM) starter notch. The desired final fatigue flaw shape ratio ( $a/2c$ ) was 0.40 to 0.50. The initial EDM notch size was determined by sizing the final fatigue flaw and then subtracting off the desired flaw extension (i.e., generally in the range of 0.005 to 0.050 inches depending on the flaw size), taking account of the observation that the depth growth-to-width growth ratio ( $\Delta a/\Delta c$ ) has a specific value. For center cracks and edge cracks in 2014-T6 aluminum,  $\Delta a/\Delta c$  was about 1.8. For center cracks in 6Al-4V titanium-STA,  $\Delta a/\Delta c$  was equal to 2.1 and for A533B steel,  $\Delta a/\Delta c$  was approximately 1.3. For the 2014-T6 strain gradient specimen, the growth ratio,  $\Delta a/\Delta c$ , was assumed to be the product of 1.8 (growth ratio for edge cracks in uniform stress field) and the ratio of elastic stress concentration at the edge of the hole-to-elastic stress concentration at the location of the notch tip. For hole diameters ranging from 1/8 to 3/4 in., the hole edge-to-notch tip ratios varied from 2.1 to 1.2. This corresponds to a variation in  $\Delta a/\Delta c$  between 3.8 and 2.2. These values came extremely close to the actual measured growth ratios.

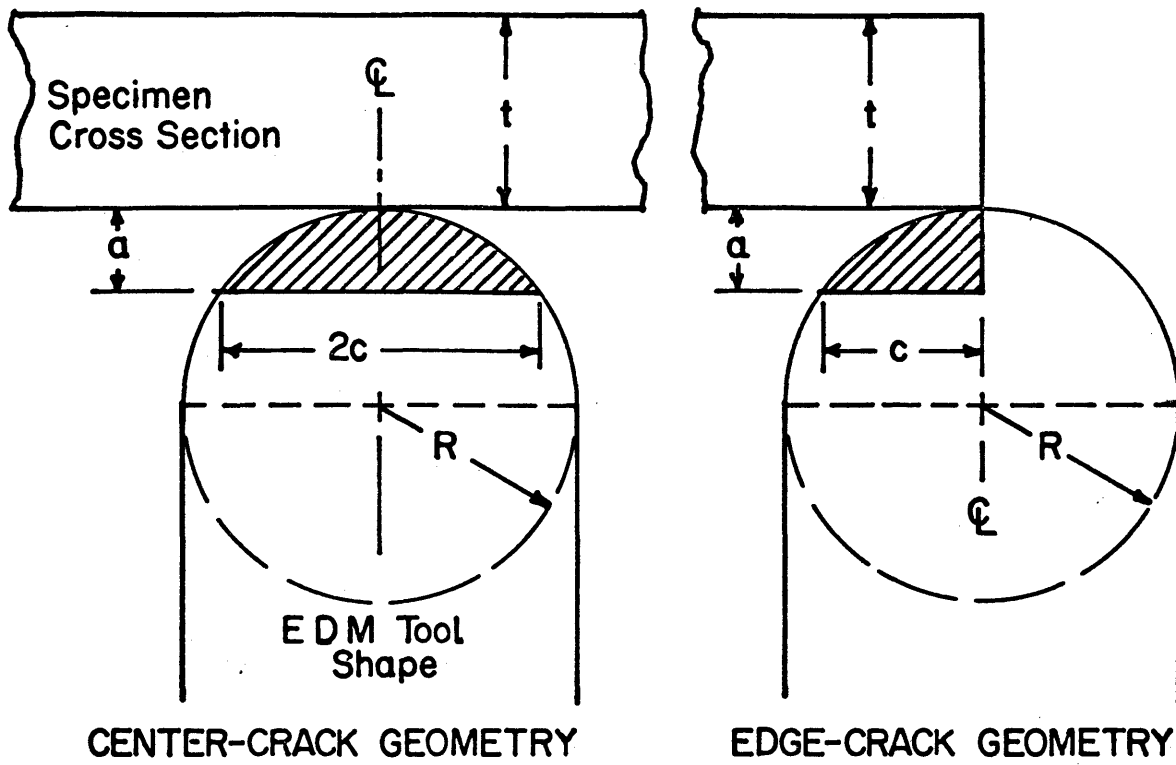
A 0.010-in.-thick tungsten-copper electrode was used to machine the notch. The tool radius of the semi-circular electrode was determined using simple geometry, as shown in Figure 5. For center crack and edge crack specimens, the tool radius ( $R$ ) was calculated from Equation (A), Fig. 5, for a known notch depth ( $a$ ) and length ( $2c$ ). For circular hole-edge crack specimens, Equation (C) was solved for  $d$  or  $a$  using the quadratic formula, by substituting known values of hole radius ( $r$ ), effective preflaw depth ( $a-d$ ), and effective preflaw length ( $c-r$ ). Tool radius ( $R$ ) was determined as before from Equations (A) or (B). The EDM electrode was sharpened to a tip radius of no greater than 0.0015 in. by hand.

The maximum stress used during fatigue extension was equal to approximately 45 percent of the room temperature yield strength, or 30 ksi for 2014-T6 aluminum, 70 ksi for 6Al-4V titanium-STA, and 30 ksi for A533B steel. Surface growth ( $\Delta c$ ) was monitored with a measuring microscope.

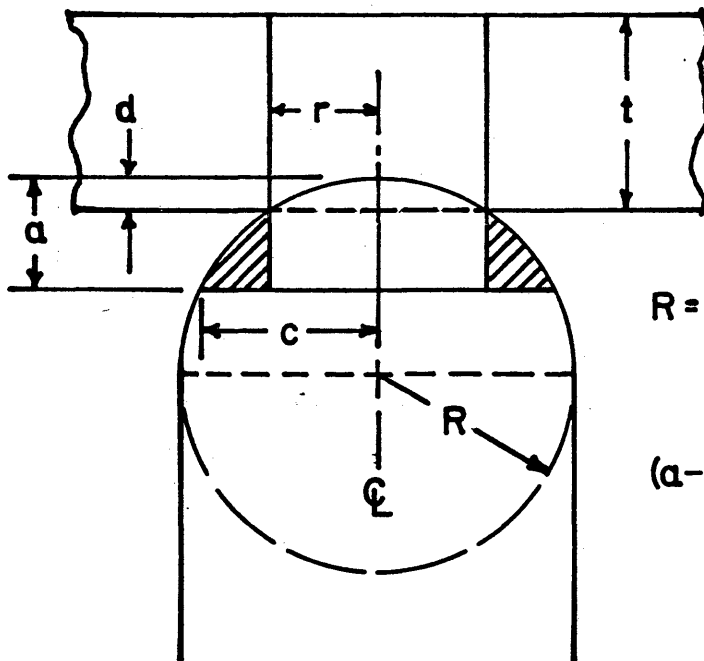
#### Strain Tolerance Measurement

After surface flaw introduction, specimens were instrumented with foil strain gages for accurate measurement of material strain tolerance.

The center-crack strain tolerance, center-crack thickness restraint, and edge-crack geometry specimens were instrumented with four strain gages for the purpose of measuring



$$R = \frac{a^2 + c^2}{2a} \quad (A)$$



$$R = \frac{d^2 + r^2}{2d} \quad (B)$$

$$(a-d)da = ar^2 - dc^2 \quad (C)$$

CIRCULAR HOLE  
EDGE CRACK GEOMETRY

Figure 5. EDM Tool Shape for Center Crack, Edge Crack, and Circular Hole-Edge Crack Geometries.

ARTHUR LAKES LIBRARY  
COLORADO SCHOOL OF MINES  
GOLDEN, COLORADO

nominal strain parallel to the loading axis. Two gages were placed in the plane of the flaw at least five half-crack lengths ( $5c$ ) away from the crack tip when failure was elastic, and ten half-crack lengths ( $10c$ ) away from the crack tip when failure was plastic. For center crack samples, these gages were at the specimen edge, and for edge crack samples, the gages were at the specimen center. The other two gages were located at the same distance, but were offset one-inch from the crack plane. Gage placement is schematically illustrated in Figure 4. Since net section-to-gross section ratios are 0.98 or greater, on-plane and off-plane gage readings ought to be very close. If they are not close, specimen width was insufficient for valid nominal strain measurement. On-plane and off-plane strains do not differ by more than 0.001 in./in. (0.1 percent) for the strain tolerance data presented in this report. The active grid of the gage used was 0.125-in. long by 0.090-in.-wide. A smaller gage was not necessary since strain was essentially uniform at  $10c$  from the crack tip. The gages used for 2014-T6 aluminum and 6Al-4V titanium-STA were made of constantan foil with an elongation capability of 5 percent strain, while those used for A533B steel were made of annealed constantan foil with an elongation capability of 20 percent strain. In addition to strain gage measurements, strain tolerance was also estimated from a photogrid with 0.100-in.-

spacing, for comparison. These photogrid strain tolerance values are not as direct as those from strain gages since the total strain is the sum of the measured plastic failure strain and the elastic strain calculated from failure stress.

The determination of the effect of a strain concentration gradient on the strain tolerance of 2014-T6 aluminum necessitated measurements from two geometrically identical specimens. The first contained the circular hole-edge crack geometry used for measurement of nominal failure strain and net section failure stress under the influence of the strain concentration gradient. The second contained the circular hole by itself, used for measurement of the plastic strain distribution at the flaw location as a function of net section stress. The active grid of the gage used to measure nominal strain at the specimen edge was 0.125-in. long by 0.090-in. wide. This gage was made from constantan foil with an elongation capability of 5 percent strain. Progressively smaller gages were used to measure strain as the edge of the hole was approached because of the progressively steeper strain gradient. The active grid of the gages intermediate between sample edge and hole edge was 0.031-in. long by 0.032-in. wide, and for those close to the edge of the hole was 0.015-in. long by 0.020-in. wide. The peak strain was measured by a gage on the inside surface of the hole. These smaller gages were made of annealed constantan

foil with an elongation capability of 10 percent strain.

All strain gages were bonded to the specimens with Micro-Measurements AE-15 heat-curing epoxy cement having an elongation capability of 20 percent strain. The gages were cured at 150°F for 2 to 3 hours under a clamping pressure of approximately 15 to 20 psi. If a photogrid was to be applied to the gage section, it was done before strain gage installation. The gage section was first sprayed with a photosensitive coating, such as Kodak metal etch resist (KMER). The coating was then exposed to ultraviolet light through a black and white negative transparency containing the grid. After exposure, the coating was developed in KMER developer and then stained with a blue dye.

After strain gage installation, the specimens were tested to tensile failure at a strain rate of approximately 0.01 in./in./min. Strain gage and load cell outputs were measured every 10 seconds during the test with a null-balance type digital strain indicator containing automatic switching, sensing, and recording units that could scan up to 20 channels of data per second. Strain tolerance for the center-crack and edge-crack specimens was taken as the average of 4 nominal strain readings at failure (2 strain gages were located on the crack plane and 2 strain gages were located off the crack plane as is illustrated in Figure 4). Effective strain tolerance for the strain concentration

gradient specimens was taken as the average of 2 nominal strain readings at failure (both strain gages were located on the crack plane as is illustrated in Figure 4).

## RESULTS AND ANALYSIS

Experimental strain tolerance results will be discussed as follows:

- (1) Baseline center-crack strain tolerance for 2014-T6 aluminum (heat 6670), 6Al-4V titanium-STA, and A533B steel.
- (2) Material variation effect on strain tolerance of 2014-T6 aluminum (heat 5867).
- (3) Thickness restraint effect on strain tolerance of 2014-T6 aluminum (heat 6670).
- (4) Edge-crack flaw geometry effect on strain tolerance of 2014-T6 aluminum (heat 6670).
- (5) Circular-hole strain gradient effect on strain tolerance of 2014-T6 aluminum (heat 6670).

### Baseline Strain Tolerance

Strain tolerance data for 2014-T6 aluminum (heat 6670), 6Al-4V titanium-STA, and A533B steel are given in Appendix A and plotted (open circles) as a function of crack depth in Figures 6, 7, and 8, respectively. The failure region marked "brittle" is a region of negligible plastic flow over which linear elastic fracture mechanics is applicable. The failure region marked "frangible" is a region of gross

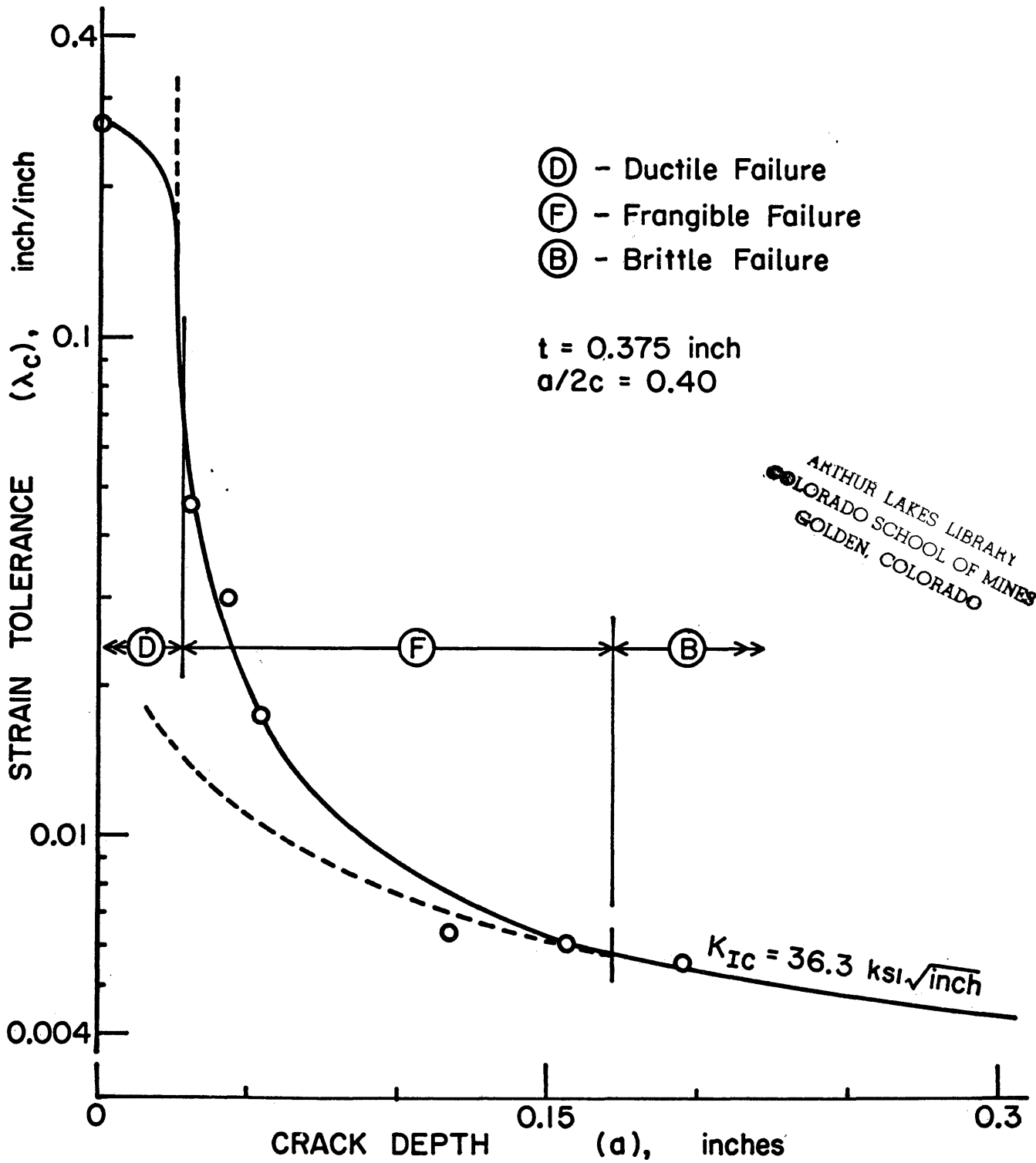


Figure 6. Strain Tolerance Curve for 2014-T6 Aluminum (Heat 6670) at Room Temperature.

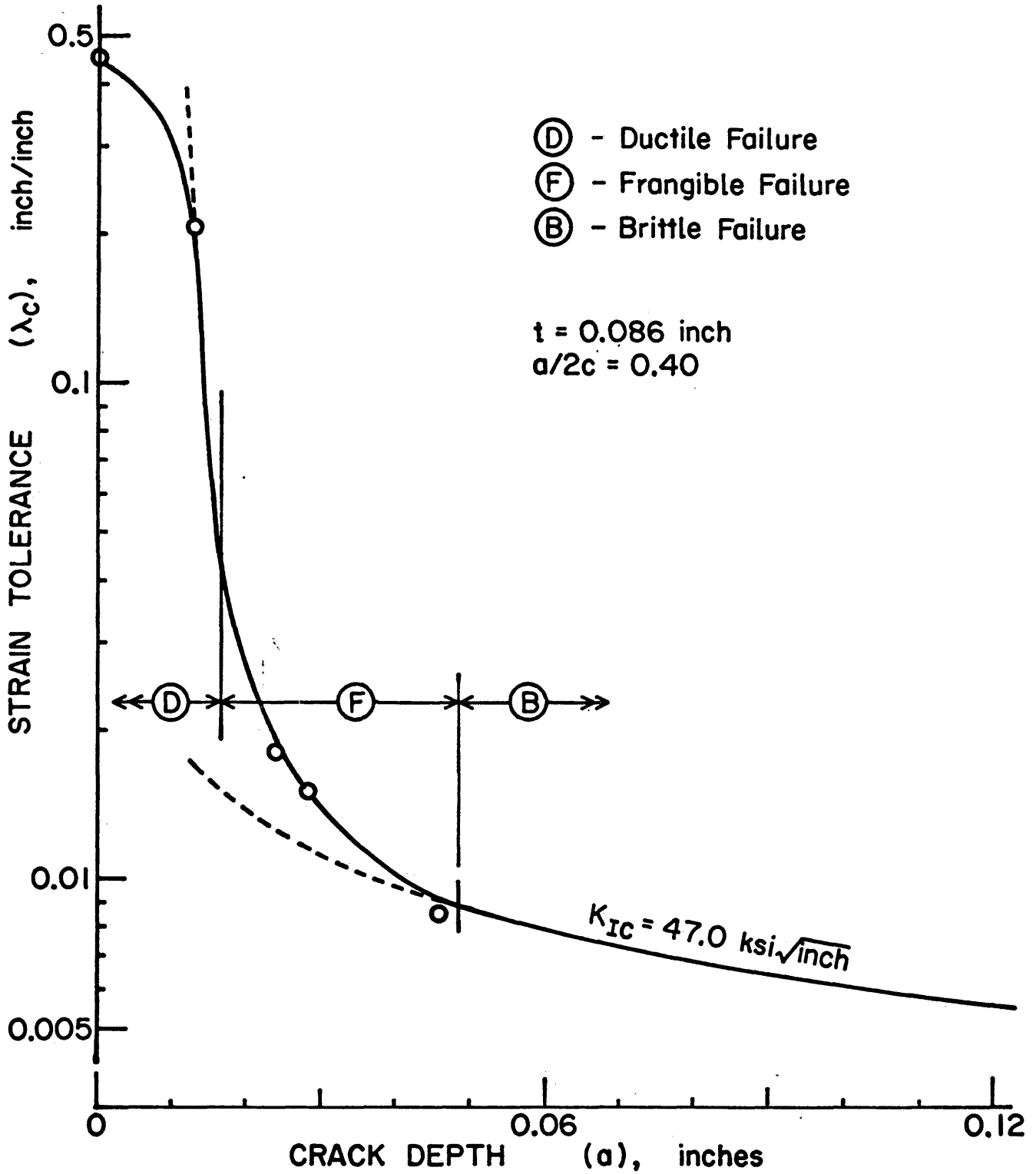


Figure 7. Strain Tolerance Curve for 6Al-4V Titanium-STA at Room Temperature.

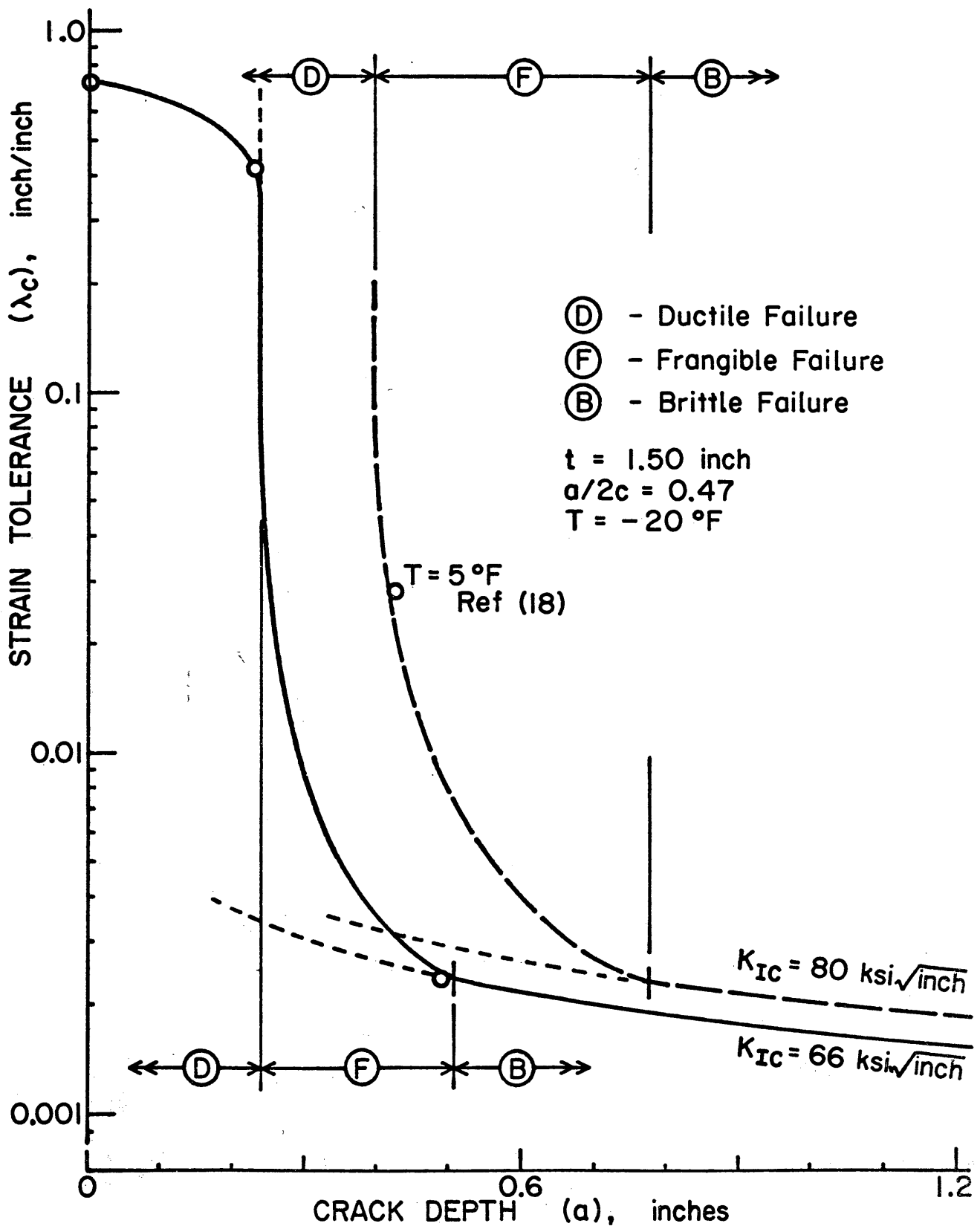


Figure 8. Strain Tolerance Curves for A533B Steel (HSST Plate 01) at  $-20$ °F and  $5$ °F.

plastic flow over which strain tolerance increases rapidly with decreasing flaw size. The failure region marked "ductile" is a region of plastic instability characterized by local necking. The brittle-frangible boundary is arbitrarily located at the point where the first measurable plastic flow starts. This corresponds to a plastic strain of approximately 0.0002. The frangible-ductile boundary is located at the point of plastic instability, which corresponds to the ultimate stress point in a tensile test. The limiting value of strain tolerance at zero crack size corresponds to the ductility in a tensile test, as calculated from reduction in area.

For 2014-T6 aluminum (heat 6670), strain tolerance increases from 0.44 percent for a 0.300-in.-deep flaw in the elastic region to 5.6 percent for a 0.030-in.-deep flaw in the plastic region, and reaches a limiting value of 26.8 percent at zero flaw size. For 6Al-4V titanium-STA, strain tolerance increases from 0.69 percent for a 0.080-in.-deep flaw in the elastic region to 2.6 percent for a 0.020-in.-deep flaw in the plastic region, and reaches a limiting value of 45.4 percent at zero flaw size. Limited data for A533B steel at  $-20^{\circ}\text{F}$  suggest that strain tolerance increases from 0.16 percent for a 1.10-in.-deep flaw in the elastic region to 5.0 percent for a 0.24-in.-deep flaw in the plastic region, and reaches a limiting value of 71.5 percent at zero

flaw size. Also plotted in Figure 8, for comparison, is a result of Loechel<sup>(18)</sup> for A533B steel (HSST-Plate 01) at 5°F using a brittle weld bead-on-plate surface flaw geometry. The shift of the strain tolerance curve to higher values with increasing temperature is reasonable.

For engineering design applications, it would be useful to have the strain tolerance versus crack size curve in the form of an equation. In the elastic region the strain tolerance versus flaw size equation is determined by expressing the linear elastic fracture mechanics stress intensity equation for a surface flaw<sup>(13)</sup> in terms of total fracture strain as

$$\lambda_c = \frac{\sqrt{Q} K_{Ic}}{1.1\sqrt{\pi} E} \sqrt{a}, \quad (1)$$

where  $Q$  is the flaw shape parameter,  $K_{Ic}$  is the fracture toughness, and  $E$  is the elastic modulus. Elastic calculations for 2014-T6 aluminum (heat 6670), 6Al-4V titanium-STA, and A533B (-20°F) are outlined in Appendix B. In the plastic region (up to the point of necking instability), the rapid increase in strain tolerance can be taken into account by the use of a plastic strain multiplying factor such as  $(1+n\epsilon_c)$ , where  $\epsilon_c$  is the plastic part of the strain tolerance and  $n$  is an empirical constant to be determined by a best-fit of the experimental data points. Rewriting Equation (1) in these terms, we have

ARTHUR LAKES LIBRARY  
 COLORADO SCHOOL OF MINES  
 GOLDEN, COLORADO

$$\lambda_c = \left[ \frac{\sqrt{Q} K_{Ic}}{1.1\sqrt{\pi} E} \cdot \frac{1}{\sqrt{a}} \right] (1+n\epsilon_c). \quad (2)$$

The relationship between total strain ( $\lambda$ ) and plastic strain ( $\epsilon$ ) can be determined from a tensile test. For a stress-strain curve expressed in the form of a power function, the relationship is

$$\lambda = \frac{B}{E} \epsilon^m + \epsilon, \text{ for } \epsilon > 0, \quad (3)$$

where  $m$  is the strain hardening exponent, and  $B$  is the stress constant at unit strain. Plastic calculations are outlined in Appendix C. Results for 2014-T6 aluminum (heat 6670), 6Al-4V titanium-STA, and A533B steel at  $-20^\circ\text{F}$  and  $5^\circ\text{F}$  are shown in Table 3. The accuracy of the strain tolerance curve in the frangible region may be only  $\pm 5$  percent because strain is changing so rapidly with crack depth. Improved accuracy would require a statistical error analysis of a larger amount of data.

#### Material Variation Effect

Center-crack strain tolerance was determined for a second heat of 2014-T6 aluminum (heat 5867), having a yield strength of 58.3 ksi, for comparison with baseline heat 6670, having a yield strength of 66.6 ksi. Strain tolerance results are given in Table 4. Over a range of crack depths from 0.050 to 0.090 inches, the strain tolerance of heat 5867 is an average of 38 percent higher than for heat 6670.

TABLE 3 Semiempirical Equation For Strain Tolerance  
As a Function of Crack Size For 2014-T6 Aluminum (Heat 6670),  
6 Al-4V Titanium-STA, and A533B Steel

1652

Alloy Designation	Yield Strength $S_y$ (psi)	Temperature $T$ ( $^{\circ}F$ )	Flaw Shape Ratio $a/2c$	Flaw Shape Parameter $Q$	Fracture Toughness $K_{Ic}$ (ksi $\sqrt{in.}$ ) ( $psi \times 10^{-6}$ )	Elastic Modulus $E$	Empirical Constant* $n$	Empirical Constant+ $B$	Strain Hardening Exponent+ $m$
2014-T6 Aluminum	66,600	70	0.40	1.88	36.3	10.6	62	82,200	0.038
6Al-4V Titanium-STA	160,300	70	0.40	1.88	47.0	17.0	56	194,000	0.030
A533B Steel	70,800	-20	0.47	2.19	66.0	29.9	290	150,300	0.160
A533B Steel	69,000	5	0.47	2.19	80.0	29.9	310	146,300	0.160

$$\lambda_c = \left[ \frac{\sqrt{Q} K_{Ic}}{1.1 \sqrt{\pi E}} \cdot \frac{1}{\sqrt{a}} \right] (1 + n \epsilon_c)$$

Where  $\lambda = \frac{B}{E} \epsilon^m + \epsilon$ , for  $\epsilon > 0^{**}$

\*  $n$  is determined from best-fit of plastic strain tolerance data.

+  $B$  and  $m$  are determined from tensile flow curve.

\*\* Two equations are used to describe the flow curve for A533B steel as it exhibits a discontinuous yield point:  $\lambda = (S_y/E) + \epsilon$ , for  $0 < \epsilon < 0.009$

$\lambda = (B/E) \epsilon^m + \epsilon$ , for  $\epsilon \geq 0.009$

TABLE 4 Strain Tolerance Data for 2014-T6 Aluminum (Heat 5867)

at Room Temperature

Specimen Number	Thickness t (in.)	Width W (in.)	Gross Area $A_g^2$ (in. <sup>2</sup> )	Flaw Depth a (in.)	Flaw Length 2c (in.)	Depth Ratio a/t	Shape Ratio a/2c	Net Area $A_n^2$ (in. <sup>2</sup> )	Area Ratio $A_n/A_g$
A3	0.379	3.235	1.226	0.058	0.143	0.153	0.406	1.219	0.994
A4	0.364	3.244	1.181	0.088	0.204	0.242	0.431	1.167	0.988
A5	0.362	3.240	1.173	0.062	0.167	0.171	0.371	1.165	0.993

TABLE 4 (Continued)

Specimen Number	Fracture Load $P_f$ (lb)	True Total Fracture Strain $\lambda_f$ (in./in.)	True Fracture Stress $S_n$ (psi)	Stress Ratio $S_n/S_y$	Strain Tolerance Heat 6670 $\lambda_c$ (in./in.)	Strain Ratio $\lambda_f/\lambda_c$
A3	79,250	0.0249	66,200	1.14	0.0156	1.60
A4	72,500	0.0124	62,500	1.07	0.0100	1.24
A5	72,600	0.0187	63,100	1.08	0.0144	1.30

True Yield Stress = 58,300 psi

Elastic Modulus =  $10.6 \times 10^6$  psi

True Ultimate Stress  $\approx$  71,200 psi

Fracture Toughness = 39.9 ksi  $\sqrt{\text{in.}}$

True Ultimate Strain  $\approx$  0.0700

ARTHUR LAKES LIBRARY  
COLORADO SCHOOL OF MINES  
GOLDEN, COLORADO

It is apparent that differences in the tensile flow properties for these two heats is also indicative of their different strain tolerance behavior in the presence of flaws. In engineering design where weight-savings are of primary concern, it therefore becomes important to determine actual strain tolerance values for the particular heat of material to be used in the application. If this approach becomes prohibitively expensive, then design must be based on lower-bound values for a particular alloy.

#### Thickness Restraint Effect

Baseline strain tolerance data for 2014-T6 aluminum (heat 6670), shown in Figure 6, was determined using a section size nominally 0.375-in. thick and 3.5-in. wide. For maximum utility in hardware design, it is hoped that strain tolerance will have a minimum value corresponding to "full restraint", in the plastic region, similar to "plane strain fracture toughness", in the linear elastic region. If this is true, then strain tolerance should increase with decreasing width and thickness below that required for "full restraint".

The width criteria for valid strain tolerance measurements, namely that ligament width be equal to 10 times the half-crack length ( $W_0 \geq 10c$ ), may also be a necessary and sufficient criteria for "full width restraint". This seems reasonable as a hypothesis, since the width restraint is at

least sufficient to cause the local plastic strain distribution at the crack tip to die out to the nominal strain before reaching the specimen boundaries. If this is the case, then "full thickness restraint" should also be present when the ligament thickness is equal to 10 times the crack depth ( $t_l \geq 10a$ ). For the largest size flaw tested that still caused plastic failure ( $a = 0.054$ ,  $2c = 0.126$ ), the ligament width was equal to 26.8 times the half-crack length ( $W_l = 26.8c$ ) and the ligament thickness was equal to 6.0 times the crack depth ( $t_l = 6.0a$ ). If the hypothesis is correct, then the 2014-T6 strain tolerance sample has full restraint in the width direction but has something less than full restraint in the thickness direction.

Limited tests were performed to determine the effect of thickness on strain tolerance. Test results for two thicknesses, 0.089 and 0.145 inches, are compared with baseline strain tolerance results for 0.375-in. thickness in Table 5. The flaw size was kept constant. Ligament thickness-to-flaw depth ratios ( $t_l/a$ ) for thicknesses of 0.375, 0.145, and 0.089 inches are equal to 6.0, 1.7, and 0.7, respectively. The nominal fracture strain for the 0.145-in. thickness is 46 percent lower, and for the 0.089-in. thickness is 60 percent lower, than the strain tolerance for the 0.375-in. thickness. This result is exactly opposite to what was expected, indicating that the lower restraint at these

TABLE 5 Thickness Restraint Effect on Strain Tolerance of  
2014-T6 Aluminum (Heat 6670)

Specimen Number	Thickness t (in.)	Width W (in.)	Gross Area $A_g^2$ (in. <sup>2</sup> )	Flaw Depth a (in.)	Flaw Length 2c (in.)	Depth Ratio a/t	Shape Ratio a/2c	Net Area $A_n$ (in. <sup>2</sup> )	Area Ratio $A_n/A_g$
A10	0.376	3.501	1.316	0.054	0.126	0.144	0.429	1.311	0.996
A13	0.145	3.502	0.5078	0.054	0.130	0.372	0.415	0.5023	0.989
A14	0.089	3.501	0.3116	0.053	0.127	0.596	0.417	0.3063	0.983

TABLE 5 (Continued)

Specimen Number	Fracture Load $P_f$ (lb)	True Total Fracture Strain $\lambda_f$ (in./in.)	True Fracture Stress $S_n$ (psi)	Stress Ratio $S_n/S_y$	Strain Tolerance $\lambda_c$ (in./in.)	Strain Ratio $\lambda_f/\lambda_c$	Back Surface Strain $\lambda_b$ (in./in.)
A10	88,280	0.0172	68,000	1.02	0.0172	1.00	0.0178
A13	33,650	0.0093	67,200	1.01	0.0172	0.54	0.0124
A14	20,190	0.0068	65,900	0.99	0.0172	0.40	0.0132

True Yield Stress = 66,600 psi  
 True Ultimate Stress = 74,800 psi  
 True Ultimate Strain = 0.0733

Elastic Modulus =  $10.6 \times 10^6$  psi  
 Fracture Toughness =  $36.3 \text{ ksi}\sqrt{\text{in.}}$

thicknesses was overshadowed by another effect. Apparently, at flaw depth ratios ( $a/t$ ) equal to as little as 0.35 and greater, there is a stress intensity magnification effect by virtue of the ligament thickness being too thin.

Note that the back-surface strain, measured in the plane of the flaw, for the 0.375-in. thickness ( $t_\ell/a = 6.0$ ) is only 4 percent higher than the strain tolerance, while for the 0.145-in. thickness ( $t_\ell/a = 1.7$ ) and for the 0.089-in. thickness ( $t_\ell/a = 0.7$ ), it is 33 percent and 94 percent higher, respectively. This result indicates that the ligament-dimension criteria for nominal strain measurement in the thickness direction is something greater than 6 times the crack depth, though not necessarily as high as 10 times the crack depth as was true with respect to width.

More testing is needed to definitely establish the effect of thickness restraint on strain tolerance, especially at ligament thickness-to-crack depth ratios greater than 6. It is probable that strain tolerance may still have a minimum value at full restraint and may increase with decreasing thickness over a limited range of lower restraints, since the ligament thickness is still sufficiently large so that the stress intensity magnification effect is negligible. However, as thickness is decreased further, the strain tolerance will pass through a maximum and rapidly decrease due to the increased domination of the stress intensity magnification effect at low ligament thicknesses.

Until the effect of thickness restraint is more completely understood, it will be necessary, when using the strain tolerance approach in hardware design, to make the strain tolerance specimen thickness identical to that expected in the hardware.

#### Flaw Geometry Effect

The effect of an edge-crack geometry (quarter-elliptical corner flaws) on the baseline center-crack strain tolerance (semielliptical surface flaw) of 2014-T6 aluminum (heat 6670) was determined because the strain gradient specimens contained quarter-elliptical corner flaws at the edges of a through-thickness circular hole. In the elastic range, for through-flaws with  $2a/W \leq 0.04$ , edge cracks are 11 percent more severe than center cracks when compared on the basis of nominal fracture strain<sup>(15)</sup>. Test results for surface flaws in the plastic range ( $2c/W \approx 0.03$ ) are given in Table 6. Over a range of flaw depths from 0.030 to 0.050 inches, the nominal fracture strain for edge cracks is an average of 22 percent less than the strain tolerance for center cracks. From these results, it appears that the severity, of edge flaws as compared with center flaws, in the plastic case is a factor of two higher than in the elastic case.

#### Strain-Gradient Effect

The determination of the effect of a strain concentration gradient on the strain tolerance of 2014-T6 aluminum

TABLE 6 Edge-Crack Flaw Geometry Effect on Strain Tolerance  
Of 2014-T6 Aluminum (Heat 6670)

Specimen Number	Thickness t (in.)	Width W (in.)	Gross Area $A_g$ (in. <sup>2</sup> )	Flaw Depth a <sub>1</sub> (in.)	a <sub>2</sub> (in.)	Flaw Length c <sub>1</sub> (in.)	c <sub>2</sub> (in.)	Depth Ratio a/t	Shape Ratio a/c	Net Area $A_n$ (in. <sup>2</sup> )	Area Ratio $A_n/A_g$
A15	0.375	3.502	1.313	0.030	0.032	0.038	0.036	0.083	0.838	1.311	0.998
A16	0.375	3.501	1.313	0.048	0.050	0.058	0.060	0.131	0.830	1.308	0.996

10-18-66

TABLE 6 (Continued)

Specimen Number	Fracture Load $P_f$ (lb)	True Total Fracture Strain $\lambda_f$ (in./in.)	True Fracture Stress $S_n$ (psi)	Stress Ratio $S_n/S_y$	Strain Tolerance $\lambda_c$ (in./in.)	Strain Ratio $\lambda_f/\lambda_c$
A15	88,620	0.0374	69,700	1.05	0.0461	0.81
A16	86,120	0.0143	66,300	0.99	0.0191	0.75



True Yield Stress = 66,600 psi      Elastic Modulus =  $10.6 \times 10^6$  psi  
 True Ultimate Stress = 74,800 psi      Fracture Toughness = 36.3 ksi  $\sqrt{\text{in.}}$   
 True Ultimate strain = 0.0733

(heat 6670) necessitated measurements from two geometrically identical specimens. One contained the circular hole by itself used for measurement of the plastic strain distribution at the flaw location as a function of net section stress. The other contained the circular hole-edge crack geometry used for measurement of nominal failure strain and net section failure stress under the influence of the strain concentration gradient.

Circular Hole Geometry Tests: Strain distribution measurements, from elastic to fully plastic, were made for four hole sizes ranging from 1/8- to 3/4-in. diameter. For a hole in a semi-infinite plate (hole diameter-to-plate width ratio ( $D/W$ ) equal to zero), the theoretical peak elastic strain concentration factor ( $K_t$ ) is equal to 3.  $K_t$  is defined as the ratio of peak strain-to-net section strain, where net section strain is equal to net section stress divided by elastic modulus. For an increasing  $D/W$  ratio greater than zero,  $K_t$  will decrease because the peak strain will be progressively less at any given value of net section strain<sup>(19)</sup>. Experimental peak elastic strain concentration factors for 0.750, 0.500, 0.250, and 0.126-in.-diameter holes, based on net section strain, are given in Table 7. Experimental  $K_t$  ranges from 2.98 for the smallest hole ( $D/W = 0.036$ ) to 2.39 for the largest hole ( $D/W = 0.214$ ). These values are within 3 percent of the theoretical values.

TABLE 7 Peak Elastic Strain Concentration Factors  
for Holes in Finite Width Plate,  
Based on Net Section Strain

Specimen Number	Thickness t (in.)	Width W (in.)	Hole Diameter D (in.)	Net Area A <sub>n</sub> (in. <sup>2</sup> )	Fracture Load P <sub>f</sub> (lb.)	Fracture Stress S <sub>n</sub> (psi)	D/W	Peak Elastic Strain Concentration Factor*	
								(K <sub>t</sub> ) <sup>+</sup> Theor.	(K <sub>t</sub> ) Expt.
A17	0.375	3.500	0.750	1.031	71,800	69,600	0.214	2.49	2.39
A18	0.374	3.501	0.500	1.122	78,600	70,100	0.143	2.62	2.59
A19	0.376	3.501	0.250	1.222	84,200	68,900	0.071	2.80	2.73
A20	0.376	3.501	0.126	1.269	86,900	68,500	0.036	2.90	2.98

\*  $K_t = \frac{\text{Peak Strain}}{\text{Net Section Strain}} = (\text{Peak Strain}) \frac{\text{Elastic Modulus}}{\text{Net Section Stress}}$

+ Reference [19]

Yield Stress = 66,500 psi      Elastic Modulus = 10.6 x 10<sup>6</sup> psi

Ultimate Stress = 70,000 psi

However, if peak strain at the hole edge is compared to nominal strain at the sample edge, the peak elastic strain concentration factor will be a constant equal to the semi-infinite plate value of 3, independent of  $D/W$  ratio. As  $D/W$  increases above zero in finite width plates, the whole strain gradient decreases proportionally (peak strain as well as nominal strain) for force equilibrium, since the strain concentration gradient exists over a significant part of the plate width. Only as  $D/W$  approaches zero and the concentration gradient becomes an insignificant part of the plate width, will the nominal strain at the sample edge approach the net section strain. Experimental elastic strain concentration gradients for 0.750, 0.500, 0.250, and 0.126-in.-diameter holes, based on nominal strain, are given in Figure 9. Note that the peak elastic strain concentration factor is independent of hole size ( $D/W$  ratio), being equal to 3.1 at the edge of the hole. Also, note that the steepness of the strain gradient is inversely proportional to hole diameter.

Peak strain and nominal strain are plotted as a function of net section stress, well into the plastic region, in Figure 10 (0.750-in.-diameter hole), 11 (0.500-in.-diameter hole), 12 (0.250-in.-diameter hole), and 13 (0.126-in.-diameter hole). The net section strain curve is identical in all four figures and provides a common reference level.

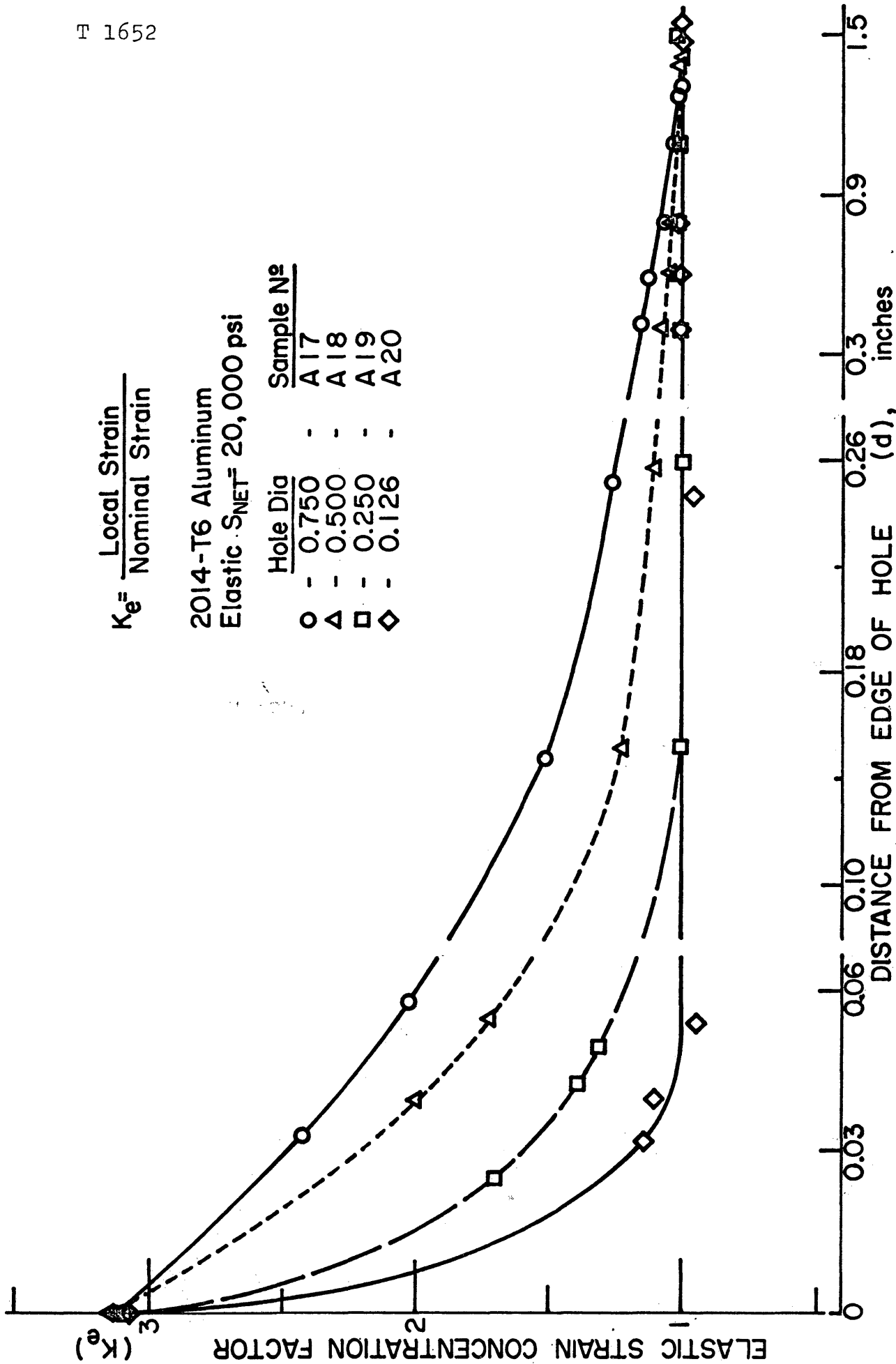


Figure 9. Elastic Strain Concentration Gradients for Holes in Finite Width Plate, Based on Nominal Strain.

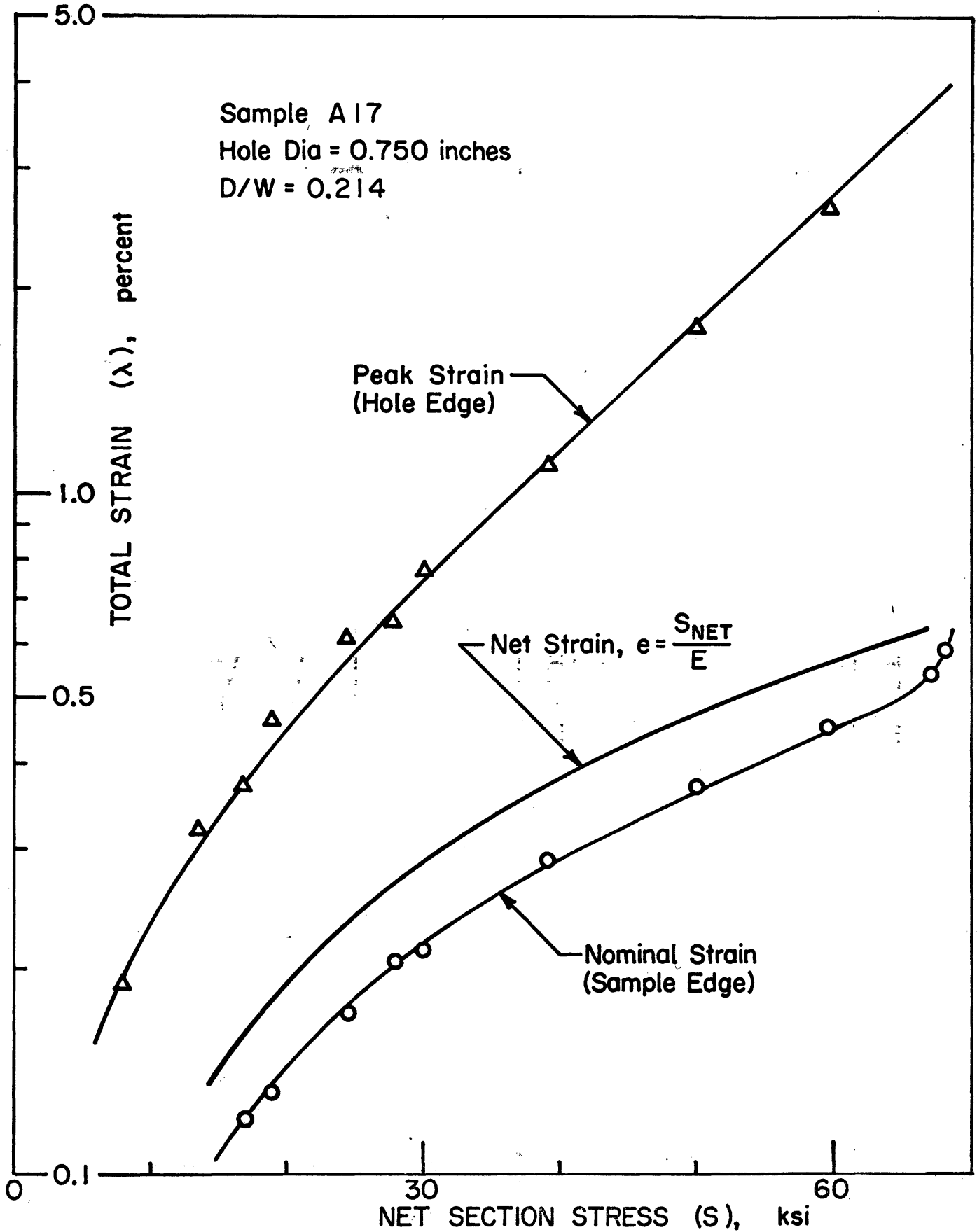


Figure 10. Peak and Nominal Strain as a Function of Net Section Stress for a 0.750-in.-Diameter Hole.

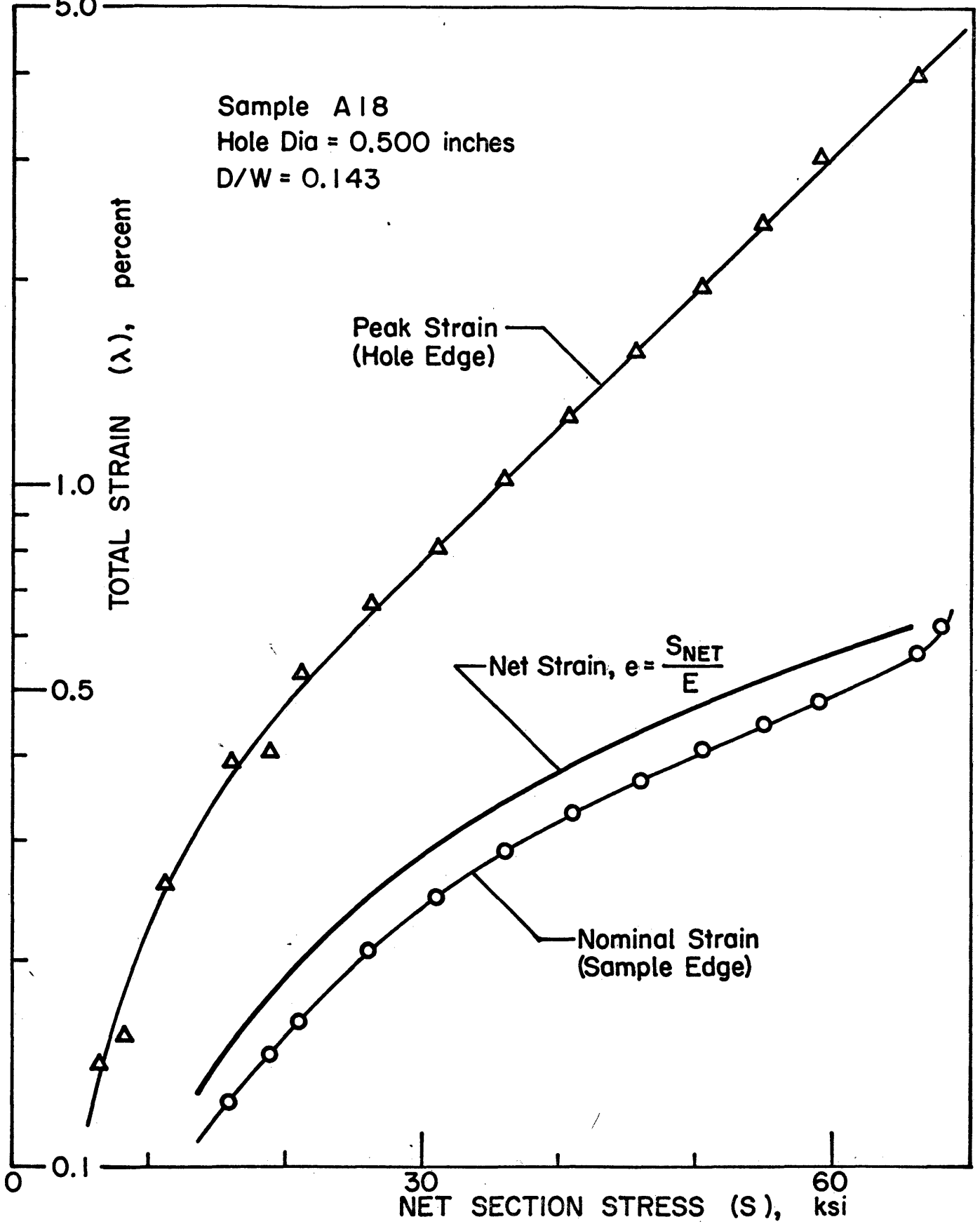


Figure 11. Peak and Nominal Strain as a Function of Net Section Stress for a 0.500-in.-Diameter Hole.

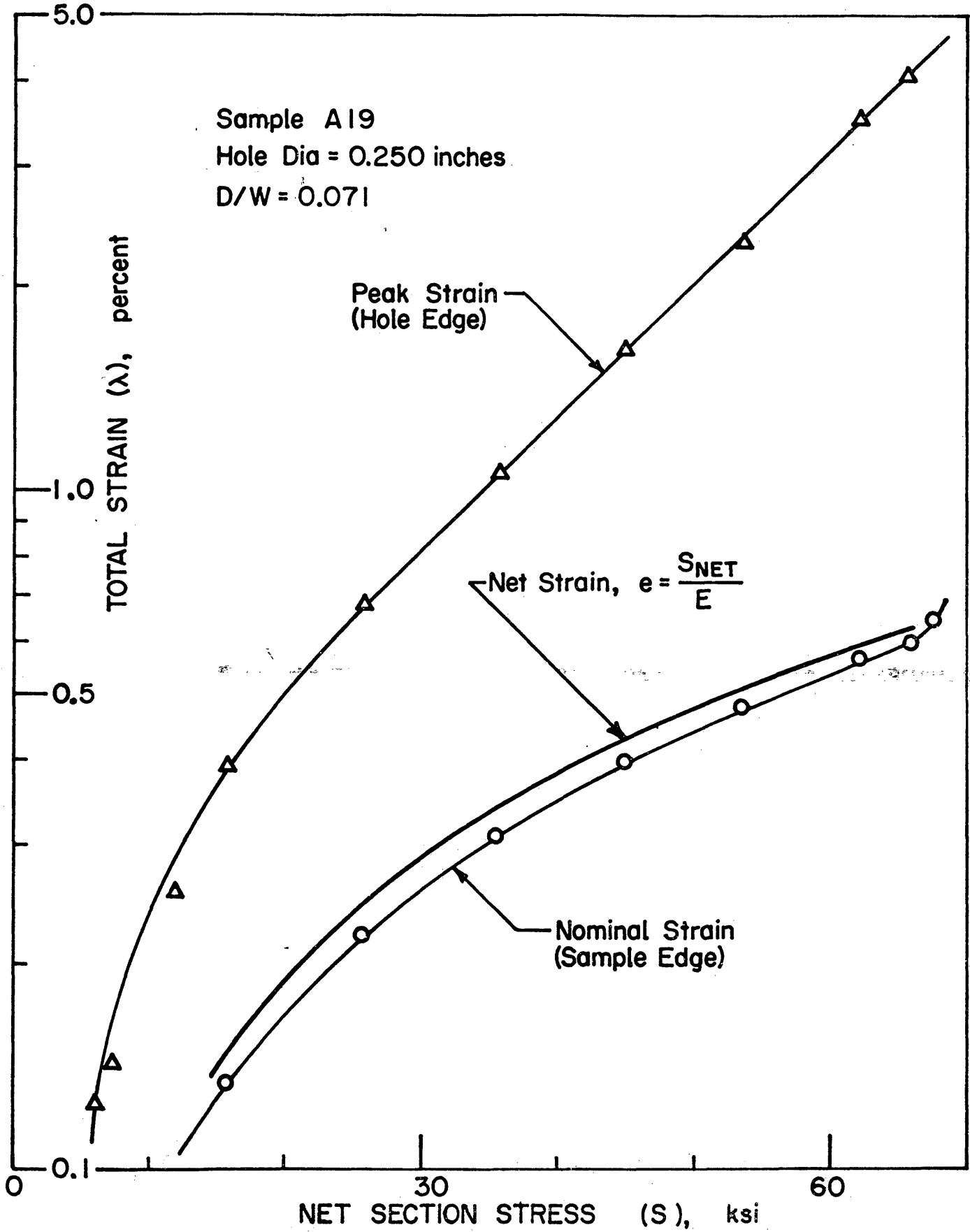


Figure 12. Peak and Nominal Strain as a Function of Net Section Stress for a 0.250-in.-Diameter Hole.

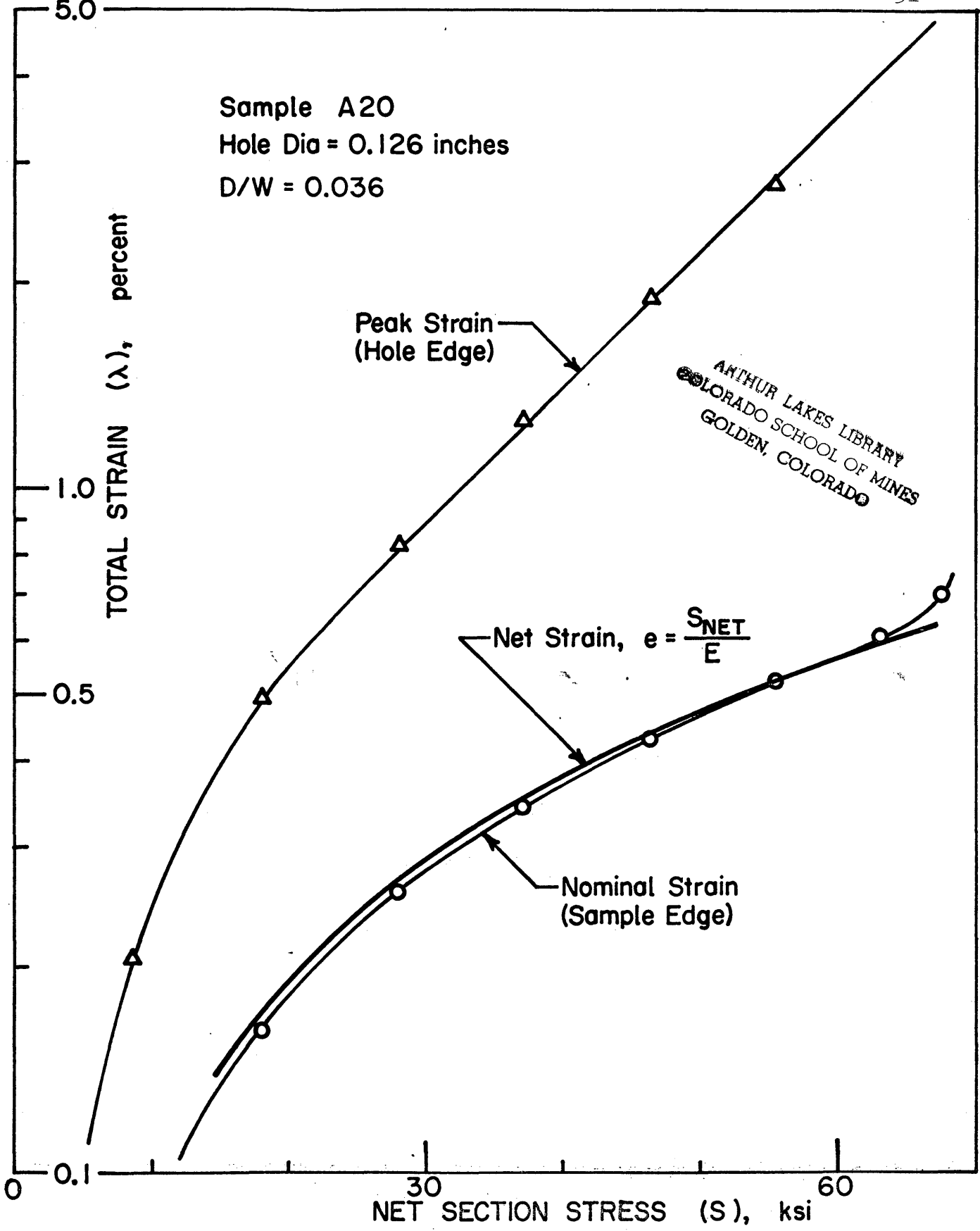


Figure 13. Peak and Nominal Strain as a Function of Net Section Stress for a 0.126-in.-Diameter Hole.

Note that as hole diameter decreases (decreasing  $D/W$ ), the nominal strain and peak strain both increase, with the nominal strain approaching the net section strain only for the smallest hole size. However, by defining the peak strain concentration factor by the ratio of peak strain-to-nominal strain, it becomes independent of  $D/W$  ratio. Up to a net section stress of 22 ksi (66 ksi yield) the section is completely elastic. At this point, the edge of the hole will flow plastically, so that peak strain will increase more rapidly with further increase in net section stress, than will nominal strain which still remains elastic. This will cause the peak strain concentration factor to increase, above its elastic value of 3, as a function of net section stress (or strain). The rate of increase will depend on the material flow properties. At a net section stress of 66 ksi, the whole section will be completely plastic, so that the nominal strain will increase at approximately the same rate as the peak strain. This will result in the peak strain concentration factor being essentially constant for the fully plastic section. In other words, the plastic strain concentration factor will have a limiting value that is only dependent on the material flow properties.

Experimental plastic strain concentration factor for 2014-T6 aluminum (heat 6670) is shown as a function of net section stress (and strain) in Figure 14. It increases from

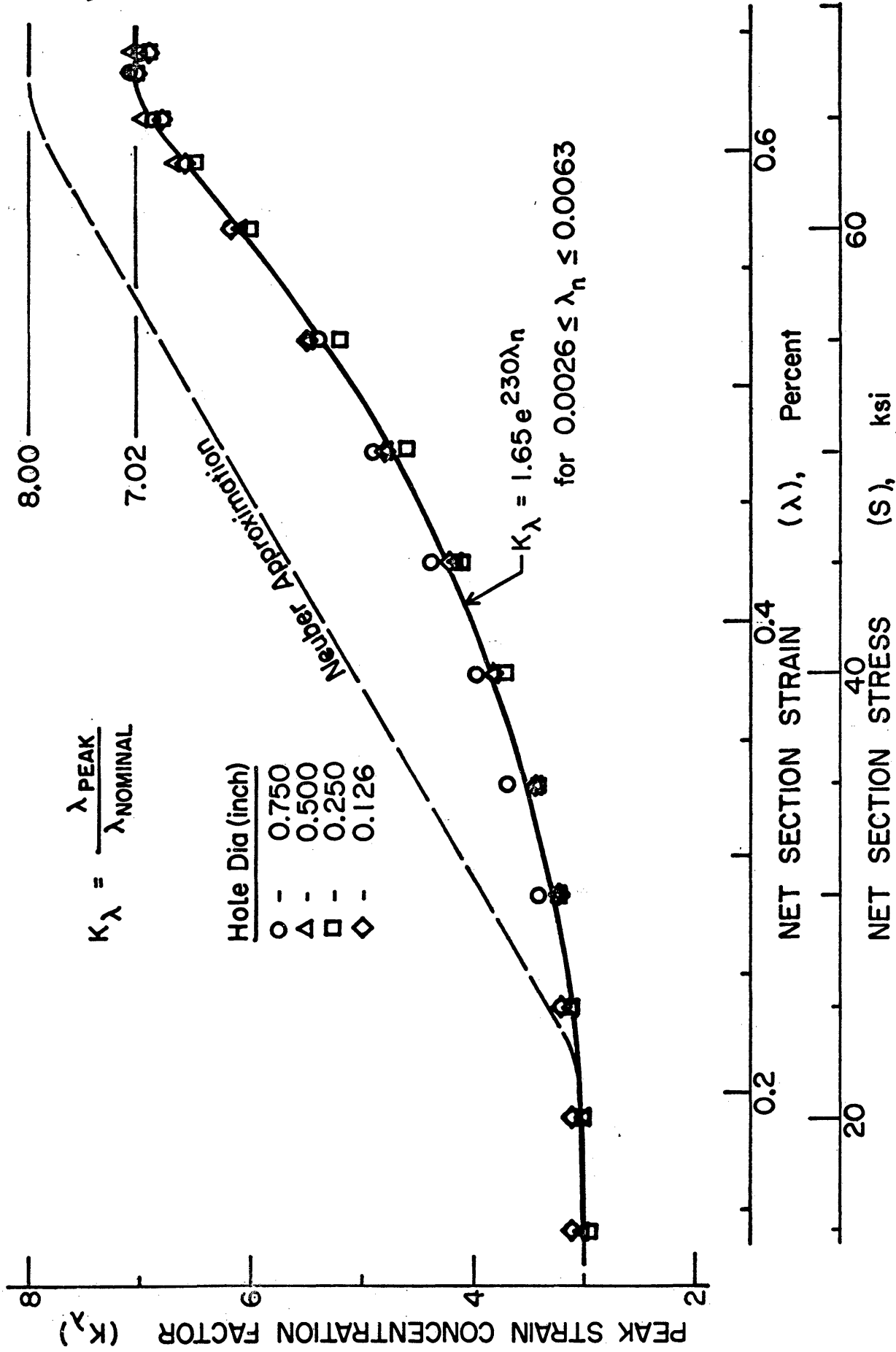


Figure 14. Peak Strain Concentration Factor, for a Circular Hole in 2014-T6 Aluminum, as a Function of Net Section Stress or Strain.

an elastic value of 3.0 to a limiting value of 7.0 when the section becomes completely plastic. Also shown is an analytical approximation for the plastic strain concentration factor originally developed by Neuber<sup>(20)</sup> for monotonic shear loading, but which has been applied by Krempl<sup>(21)</sup> and Papirno<sup>(22)</sup> to tension and compression loading. The basis of the Neuber approach is the suggested rule that the geometric mean of plastic stress concentration factor ( $K_s$ ) and the plastic strain concentration factor ( $K_\lambda$ ) is equal to the theoretical elastic concentration factor ( $K_t$ ), or

$$(K_s K_\lambda)^{1/2} = K_t, \quad (4)$$

where  $K_s$  is equal to the ratio of peak stress-to-net section stress and  $K_\lambda$  is equal to the ratio of peak strain-to-net section strain. This relationship is derived from non-linear elastic theory for sharp notches and must be regarded as being purely empirical for non-linear elastic-plastic behavior. For a material with a plastic flow curve that can be expressed in the form of a power function, the stress-strain relation at the plastic notch is

$$S_p = B \lambda_p^m, \quad (5)$$

where  $S_p$  is the peak stress,  $\lambda_p$  is the peak strain,  $m$  is the strain hardening exponent, and  $B$  is the stress constant at unit strain. The stress-strain relation in the elastic net section is

$$S_n = E \lambda_n,$$

where  $S_n$  is the nominal stress,  $\lambda_n$  is the nominal strain, and  $E$  is the elastic modulus. By substituting Equations (5) and (6) into Equation (4), the plastic strain concentration factor ( $K_\lambda$ ) can be expressed as

$$K_\lambda = K_t^{2/1+m} (E/B)^{1/1+m} \lambda_n^{1-m/1+m},$$

for  $(1/K_t)(S_y/E) \leq \lambda_n \leq S_y/E,$  (7)

where  $S_y$  is the yield strength. For the case of complete elasticity [ $\lambda_n \leq (1/K_t)(S_y/E)$ ], Equation (7) reduces to  $K_\lambda = K_t$ , and for the case of full plasticity ( $\lambda_n \geq S_y/E$ ), Equation (7) reduces to  $K_\lambda = K_t^{2/1+m}$ . Analytical calculations for a circular hole in 2014-T6 aluminum (heat 6670) plate are outlined in Appendix D. Plastic strain concentration factor, from the Neuber rule, is given by

$$K_\lambda = 3.0, \quad \text{for } \lambda_n \leq 0.0021,$$

$$\text{and } K_\lambda = 780\lambda_n^{.90}, \quad \text{for } 0.0021 \leq \lambda_n \leq 0.0063,$$

$$\text{and } K_\lambda = 8.0, \quad \text{for } \lambda_n \geq 0.0063.$$

The agreement between the analytical curve and the experimental curve is good considering that the Neuber rule is based on non-linear elastic theory.

In summary, the experimental plastic strain concentration factor for a circular hole in 2014-T6 aluminum (heat 6670) is a function of net section strain, increasing from

an elastic value of 3 to a limiting value of 7 when the section becomes completely plastic. The analytical plastic strain concentration factor for a circular hole in 2014-T6 aluminum (heat 6670), determined by Neuber's method from the theoretical elastic stress concentration factor and the material flow curve, reaches a limiting value of 8 when the section becomes fully plastic.

Circular Hole-Edge Crack Geometry Tests: In order to understand the effect of plastic strain concentration gradients on strain tolerance for surface flaws in 2014-T6 aluminum, it is advantageous to first consider the effect of elastic strain gradients on strain tolerance from existing linear elastic fracture mechanics solutions. Bowie<sup>(23)</sup> has analyzed the case of an infinite plate containing two radial, diametrically opposite, through-thickness cracks of length  $a$  originating at the edge of an internal through-thickness hole of radius  $R$ . The analysis is outlined in Appendix E. Briefly though, the elastic strain tolerance ( $e_u$ ) expression for a single central through-crack of length  $2a$  in a uniform strain field,

$$e_u = \frac{K_{Ic}}{E(\pi a)^{1/2}}, \quad (8)$$

where  $K_{Ic}$  is the fracture toughness and  $E$  is the elastic modulus, is modified for the case of two edge through-cracks of length  $a$  at the edge of a circular hole of radius  $R$  as

$$e_g = \frac{K_{Ic}}{E(\pi a)^{1/2}} (a/R)^{1/2} F(a/R), \quad (9)$$

where  $e_g$  is the nominal fracture strain in the strain gradient and  $(a/R)^{1/2} F(a/R)$  is a function that expresses the influence of the strain concentration gradient. The effective strain tolerance is equal to the ratio of nominal fracture strain in the strain gradient-to-nominal fracture strain in a uniform strain field ( $e_g/e_u$ ), or

$$e_g/e_u = (a/R)^{1/2} F(a/R). \quad (10)$$

Effective strain tolerance is plotted as a function of strain gradient ratio ( $R/(R+a)$ ) in Figure 15. For  $R/(R+a)$  equal to zero, the effective strain tolerance is equal to 1, since the crack is in a uniform strain field. As  $R/(R+a)$  increases above zero, the effective strain tolerance decreases, even though the strain gradient is still too steep to affect the crack tip, because the crack length is effectively increased by the hole diameter. As  $R/(R+a)$  increases still further (decreasing strain gradient for a larger hole), the effective strain tolerance continues to decrease because of the more severe conditions that exist when the crack tip is subjected to a progressively higher strain in the strain gradient. As  $R/(R+a)$  approaches unity, the effective strain tolerance approaches a limiting value of 0.333 for a crack that is subjected to the full strain concentration at an infinite hole. Also plotted in Figure 15 are the experimental

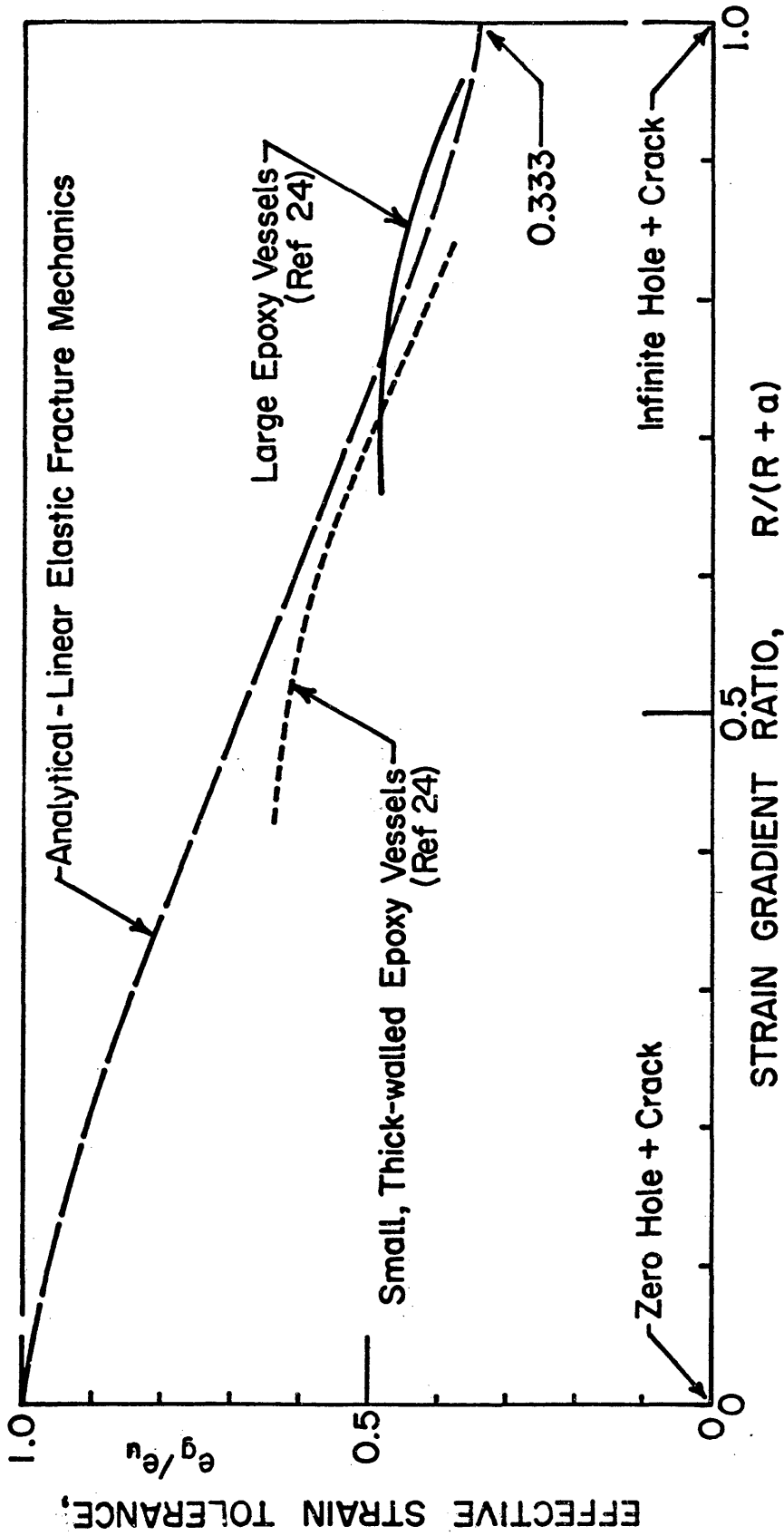


Figure 15. Elastic Strain Gradient Effect for Circular Hole-Edge Crack Geometry.

results of Derby<sup>(24)</sup> for cylindrical epoxy pressure vessels containing a quarter-circular corner crack at the edge of a circular nozzle opening in the vessel wall. The agreement with the analysis, for practical strain gradient ratios greater than 0.60, is excellent. The fact that the nominal fracture strain for a crack that is subjected to the full strain concentration is 1/3 of the nominal fracture strain in a uniform strain field is not surprising, since the theoretical elastic strain concentration factor for a hole is 3. It is probable that the effective strain tolerance in the elastic-plastic region will have a limiting value that is the reciprocal of the plastic strain concentration factor ( $K_\lambda$ ).

Experimental elastic-plastic results from the circular hole-edge crack geometry tests on 2014-T6 aluminum are given in Table 8. Nominal failure strain ( $\lambda_f$ ) and net section failure stress were measured for 0.750, 0.500, 0.250, and 0.126-in.-diameter holes containing quarter-circular corner cracks approximately 0.035-in. deep. The baseline center-crack strain tolerance ( $\lambda_c$ ) for 2014-T6 aluminum (heat 6670) is determined from Figure 6 or Table 3. The strain tolerance for edge cracks ( $\lambda_e$ ) in a uniform strain field is  $0.78\lambda_c$ , since edge cracks are 22 percent more severe than center cracks in the elastic-plastic region. Effective strain tolerance ( $\lambda_f/\lambda_e$ ) is plotted as a function of strain gradient

TABLE 8. Strain Gradient Effect on Strain Tolerance of  
2014-T6 Aluminum (Heat 6670)

Specimen Number	Thickness t (in.)	Width W (in.)	Hole Diameter D (in.)	Flaw Depth a <sub>1</sub> (in.)	a <sub>2</sub> (in.)	Net Area A <sub>n</sub> (in.)	Depth Ratio a/t	Shape Ratio a/c	Strain Gradient Ratio R/(R+a)
A21	0.376	3.502	0.750	0.032	0.035	1.033	0.089	1	0.918
A22	0.375	3.502	0.500	0.032	0.035	1.124	0.089	1	0.882
A23	0.375	3.500	0.250	0.033	0.037	1.217	0.093	1	0.781
A24	0.371	3.502	0.126	0.038	0.039	1.251	0.104	1	0.621
A25	0.375	3.500	0.250	0.033	0.036	1.217	0.092	1	0.784
A26	0.377	3.499	0.125	0.036	0.037	1.270	0.097	1	0.631

ARTHUR LAKES LIBRARY  
COLORADO SCHOOL OF MINES  
GOLDEN, COLORADO

TABLE 8. (Continued)

Specimen Number	Strain Gradient Ratio R/(R+a)	Fracture Load P <sub>f</sub> (lb)	Fracture Stress S <sub>n</sub> (psi)	Stress Ratio S/S <sub>n</sub> y	True Total Fracture Strain λ <sub>f</sub> (in./in.)	Strain Tolerance		Strain Ratio λ <sub>f</sub> /λ <sub>e</sub>
						Center Flaw λ <sub>c</sub>	Edge Flaw λ <sub>e</sub> *	
A21	0.918	67,800	65,600	0.99	0.0050	0.0413	0.0322	0.155
A22	0.882	74,200	66,000	0.99	0.0056	0.0413	0.0322	0.174
A23	0.781	79,800	65,600	0.99	0.0059	0.0368	0.0287	0.206
A24	0.621	82,300	65,800	0.99	0.0064	0.0300	0.0234	0.274
A25	0.784	80,300	66,000	0.99	0.0060	0.0382	0.0298	0.201
A26	0.631	83,000	65,400	0.98	0.0064	0.0334	0.0261	0.245

Yield Stress = 66,500 psi      Elastic Modulus = 10.6 x 10<sup>6</sup> psi

Ultimate Stress = 70,000 psi      Fracture Toughness = 36.3 ksi √in.

True Ultimate Strain = 0.0733      \*λ<sub>e</sub> = 0.78 λ<sub>c</sub>

ratio ( $R/(R+a)$ ) in Figure 16. The data indicate that the effective strain tolerance approaches a value of 0.142, which is the reciprocal of the limiting  $K_\lambda$  value of 7 (Figure 14), for a crack that sees the full strain concentration. This is not surprising since the net section in all six tests was on the verge of being fully plastic at fracture, with the net section strain approximately equal to 0.62 percent. However, since the limiting value of effective strain tolerance is a function of plastic strain concentration factor and net section strain, it is also ultimately dependent on strain tolerance and crack size. Progressively larger flaws than the average 0.035-in. depth used in the tests would have increasingly higher limiting values of effective strain tolerance. This relationship, for 2014-T6 aluminum, can be seen as follows:

The limiting value of effective strain tolerance is expressed as

$$\lambda_f/\lambda_e = 1/K_\lambda, \quad (11)$$

where  $\lambda_f$  is the nominal fracture strain in the strain concentration gradient and  $\lambda_e$  is the strain tolerance for edge cracks in a uniform strain field. But,  $\lambda_f$  is also identical to the net section strain ( $\lambda_n$ ), for small values of the  $D/W$  ratio, which is empirically related to  $K_\lambda$  from Figure 14 as

$$K_\lambda = 1.65 e^{230\lambda_n},$$

for  $0.0026 \leq \lambda_n \leq 0.0063$ . (12)

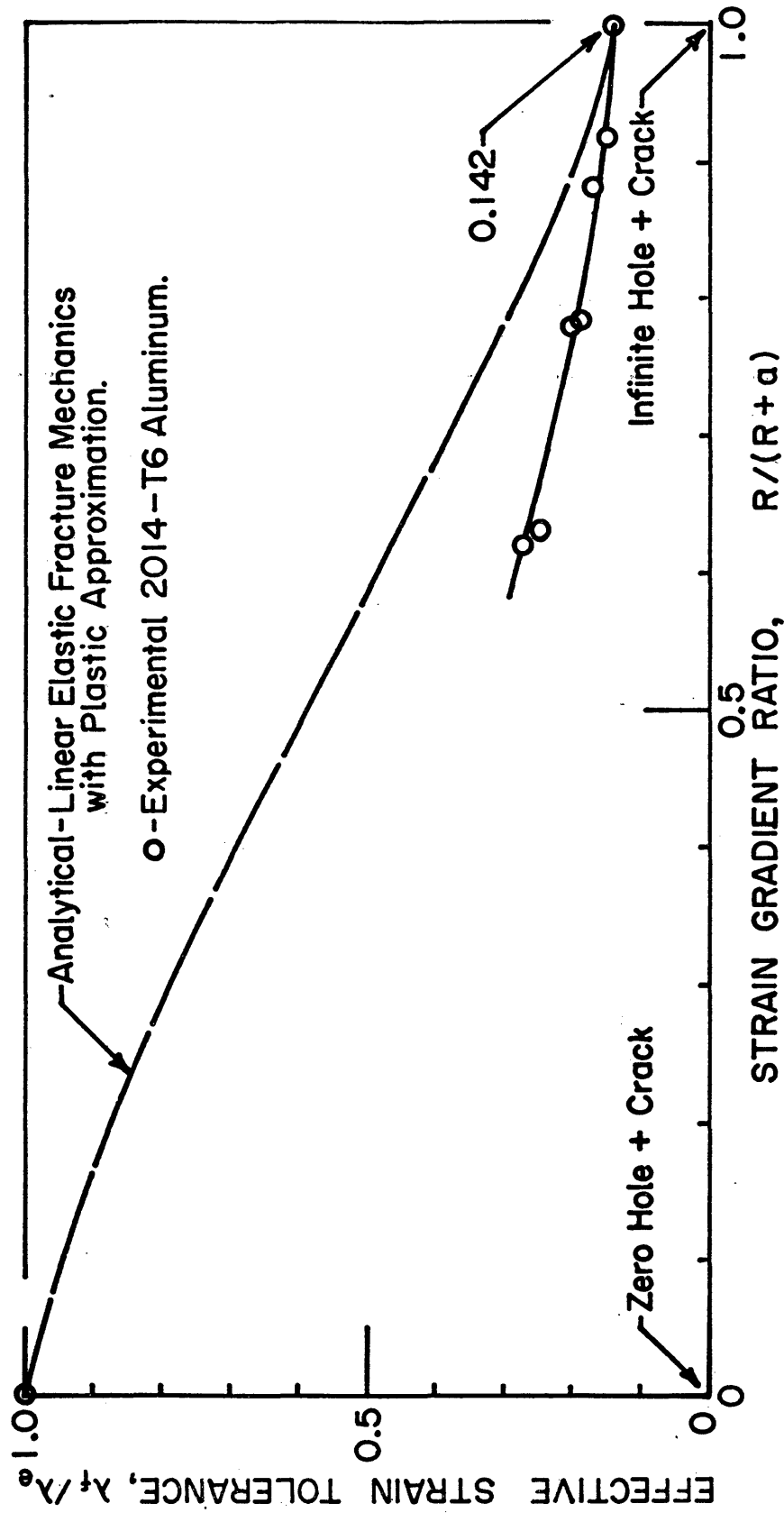


Figure 16. Plastic Strain Gradient Effect in 2014-T6 Aluminum for a Circular Hole-Edge Crack Geometry in Fully Plastic Net Section.

By combining Equations (11) and (12), the plastic strain concentration factor ( $K_\lambda$ ) can be related to the edge-crack strain tolerance ( $\lambda_e$ ) as

$$\lambda_e = \frac{K_\lambda (\ln K_\lambda - 1/2)}{230},$$

$$\text{for } 3.0 \leq K_\lambda \leq 7.0. \quad (13)$$

The complete effective strain tolerance curve in the elastic-plastic region might possibly be approximated by assuming that the effective strain tolerance  $(EST)_\lambda$  decreases between 1 and  $1/K_\lambda$  at the same rate as the elastic effective strain tolerance  $(EST)_e$  decreases between 1 and  $1/3$ . Calculations are outlined in Appendix E. The approximation equation for 2014-T6 aluminum (heat 6670), for a limiting effective strain tolerance of  $1/7$ , is

$$(EST)_\lambda = 0.214 [1 - (EST)_e] + 0.500 [3(EST)_e - 1], \quad (14)$$

where  $(EST)_e$  can be found as a function of  $R/(R+a)$  from Figure 15. The approximation curve is plotted in Figure 16 for comparison with the experimental data points. Note that the experimental effective strain tolerance is approximately 30 percent lower than the approximation curve would indicate, over the range  $0.60 \leq R/(R+a) \leq 0.90$ .

In hardware design, expression of the strain gradient effect in terms of the geometric ratio  $R/(R+a)$  limits the applicability of the results to circular hole-edge crack geometries alone, at least for steep strain gradients

( $R/(R+a) \leq 0.90$ ) that do not have the full strain concentrating effect. For shallow gradients ( $R/(R+a) > 0.90$ ), however, where the full strain concentrating effect exists, only a slightly higher degree of generality is possible, with the effective strain tolerance being equal to the reciprocal of the plastic strain concentration factor for the appropriate geometry. The plastic strain concentration factor can be calculated by Neuber's method from the appropriate theoretical elastic stress concentration factor and the material flow curve. If, on the other hand, effective strain tolerance could be expressed directly in terms of the strain gradient itself, then the results would be generally applicable to any situation for which the strain gradient is known, be it thermal stress gradients from differential heating or residual stress gradients from welding. Plastic strain concentration gradients at fracture are given in Figure 17 for the circular hole-edge crack geometry tests. These were determined from the circular hole geometry (strain distribution) tests at the appropriate value of net section failure stress. The average strain over the crack length is compared with the strain tolerance in a uniform strain field. The crack length strain is taken as the average of the peak strain at the edge of the hole and the strain at the crack tip. Note that the average strain over the crack length at fracture is approximately equal to the strain tolerance in a

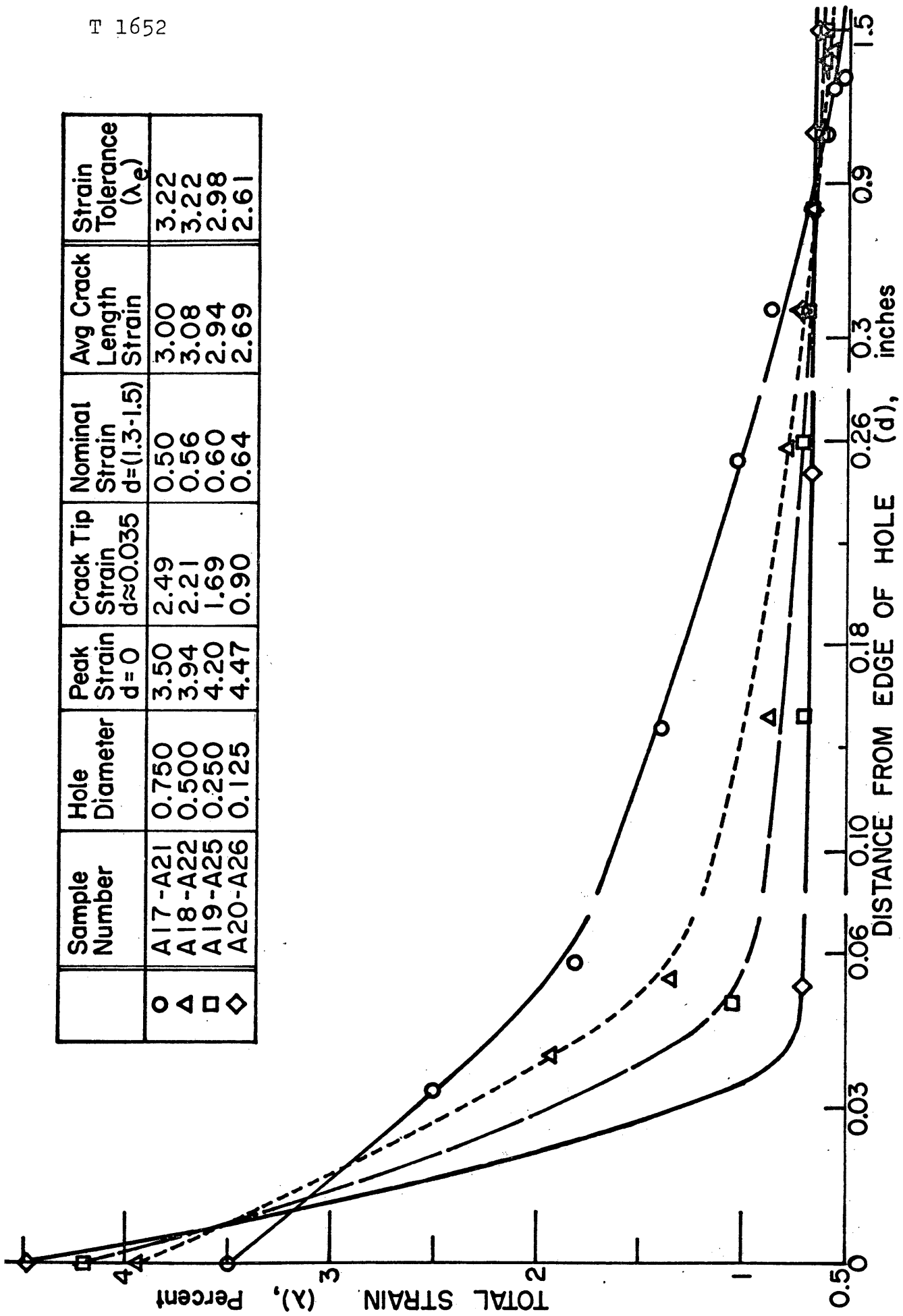


Figure 17. Plastic Strain Concentration Gradients at Fracture in 2014-T6 Aluminum for a Circular Hole-Edge Crack Geometry.

uniform strain field, within 4 percent on the average.

In summary, effective strain tolerance for a flaw in a strain concentration gradient decreases gradually with decreasing gradient steepness from a value of 1 when the flaw is in a uniform strain field, to a limiting value equal to the reciprocal of the plastic strain concentration factor when the flaw is subjected to the full strain concentrating effect. Also, the average strain over the crack length in the strain concentration gradient at fracture is approximately equal to the strain tolerance in a uniform strain field.

CONCLUSIONS

The capabilities and limitations of the strain tolerance concept as an elastic-plastic fracture criteria were analyzed in the previous section. The conclusions are the following:

- (1) The strain tolerance approach, as an elastic-plastic fracture criteria, can be applied now to the design of hardware with the reservation that strain tolerance specimen thickness is the same as in the hardware.
- (2) For 0.375-in.-thick 2014-T6 aluminum (heat 6670) at room temperature, strain tolerance increases from 0.44 percent for a 0.300-in.-deep flaw in the elastic region to 5.6 percent for a 0.030-in.-deep flaw in the plastic region, and reaches a limiting value of 26.8 percent at zero flaw size.
- (3) Strain tolerance for 0.370-in.-thick 2014-T6 aluminum (heat 5867) was 38 percent higher than for heat 6670 due to differences in their material flow properties.
- (4) For 0.086-in.-thick 6Al-4V titanium-STA at room temperature, strain tolerance increases from 0.69 percent for a 0.080-in.-deep flaw in the elastic region to 2.6 percent for a 0.020-in.-deep flaw in the plastic region, and reaches a limiting value of 45.4 percent at zero

flaw size.

- (5) Limited data for 1.50-in.-thick A533B steel (HSST Plate 01) at  $-20^{\circ}\text{F}$  suggest that strain tolerance increases from 0.16 percent for a 1.10-in.-deep flaw in the elastic region to 5.0 percent for a 0.24-in.-deep flaw in the plastic region, and reaches a limiting value of 71.5 percent at zero flaw size.
- (6) The elastic strain tolerance versus flaw size equation for a surface flaw from linear elastic fracture mechanics can be extended into the plastic region by use of a plastic strain multiplying factor and associated empirical constants.
- (7) The nominal fracture strain for edge cracks is 22 percent less than the strain tolerance for center cracks in the elastic-plastic region.
- (8) The experimental plastic strain concentration factor for a circular hole in 2014-T6 aluminum (heat 6670) is a function of net section strain, increasing from an elastic value of 3 to a limiting value of 7 when the section becomes completely plastic.
- (9) The analytical plastic strain concentration factor for a circular hole in 2014-T6 aluminum (heat 6670), determined by Neuber's method from the theoretical elastic stress concentration factor and the material flow curve, reaches a limiting value of 8 when the section becomes fully plastic.

- (10) Effective strain tolerance for a flaw in a strain concentration gradient decreases gradually with decreasing gradient steepness from a value of 1 when the flaw is in a uniform strain field, to a limiting value equal to the reciprocal of the plastic strain concentration factor when the flaw is subjected to the full strain concentrating effect.
- (11) The average strain over the crack length in the strain concentration gradient at fracture is approximately equal to the strain tolerance in a uniform strain field.

ARTHUR LAKES LIBRARY  
COLORADO SCHOOL OF MINES  
GOLDEN, COLORADO

DESIGN APPLICATION OF THE STRAIN TOLERANCEFRACTURE CRITERION

This section will illustrate the use of the strain tolerance concept in designing against defect controlled fracture in the elastic-plastic region where linear elastic fracture mechanics is not applicable. Actual strain tolerance data presented in this report will be used, and where data is not available, realistic data will be assumed. This will serve the dual purpose of making the problem practical as well as indicating what follow-on research and development is required.

Let us compute the factor of safety against burst of a 2014-T6 aluminum gaseous helium tank, for an aerospace liquid propellant pressurization system, during a room temperature proof test. The tank is a 10-in.-diameter cylinder that is 48-in. long with hemispherical ends and a wall thickness of 0.300 inches. The operating pressure is 1800 psi and the proof pressure is 2200 psi. Assume that the most severe defect that may exist in the tank is a quarter-elliptical surface flaw of shape ratio  $a/c = 0.6$ , at the edge of a 2-in.-diameter nozzle opening in the cylinder section, oriented normal to the maximum principal stress. Nondestructive inspection sensitivity is such that the maximum size flaw

that might be missed is 10 percent of the wall thickness. Elastic modulus is  $10.6 \times 10^6$  psi, Poisson's ratio is 0.3, and yield strength is 66,500 psi.

The maximum nominal principal stress in the membrane wall during proof is the tangential stress which is equal to 36,700 psi ( $Pr/t$ ). The factor of safety against general yielding in the membrane wall is  $66,500/36,700$  or 1.81. The elastic stress concentration factor for a hole in a biaxially stressed ( $S_1 = 2S_2$ ) infinite plate is equal to 2.5 which gives an apparent elastic peak stress of 91,700 psi. Since the yield strength is 66,500 psi it is apparent that the nozzle opening has yielded significantly, so that linear elastic fracture mechanics cannot be used to determine the safety factor against fracture. The first step in applying the strain tolerance approach is to find the nominal applied strain ( $\lambda_a$ ) in the structure. This can be found from the nominal membrane stresses using Hooke's Law. For a maximum principal stress ( $S_1$ ) of 36,700 psi in a thin-walled cylinder, the intermediate principal stress ( $S_2$ ) will be 18,350 psi, and the minimum principal stress will be zero. Therefore, from Hooke's Law ( $\lambda_a = (S_1 - \nu S_2)/E$ ), the nominal applied strain is equal to 0.29 percent.

The second step is to determine the nominal fracture strain ( $\lambda_f$ ) due to the strain concentration gradient for the largest defect that may be present. The maximum undetected

flaw size is 0.10t or 0.030 inches. For illustrative purposes it will be assumed that the uniaxial room temperature strain tolerance data for 0.375-in.-thick 2014-T6 aluminum ( $a/c = 0.8$ ) is not influenced by multiaxial stress\*, plate thickness\*\*, or flaw shape. For a flaw depth of 0.030 inches, the center crack strain tolerance ( $\lambda_c$ ) is 5.60 percent (Figure 6 or Table 3). The edge-crack strain tolerance ( $\lambda_e$ ) is  $0.78 \lambda_c$  or 4.36 percent (Table 6). The strain gradient ratio,  $R/(R+a)$ , is equal to 0.97. It can be seen from Figure 16 that the effective strain tolerance ( $\lambda_f/\lambda_e$ ) is essentially equal to the limiting value ( $1/K_\lambda$ ) for  $R/(R+a) \geq 0.90$ .  $K_\lambda$  can be found as a function of edge-crack strain tolerance ( $\lambda_e$ ) from empirical Equation (13). For  $\lambda_e$  equal to 4.36 percent,  $K_\lambda$  is equal to 7.0, and  $\lambda_f/\lambda_e$  is equal to  $1/7$  or 0.142. Therefore, the nominal fracture strain ( $\lambda_f$ ) is equal to  $(0.142)(4.36\%)$  or 0.62 percent. The safety factor is equal to the fracture strain ( $\lambda_f$ ) divided

---

\*Normally in both linear elastic fracture mechanics and the strain tolerance approach it is assumed that biaxiality of stress or strain has no effect on the nominal fracture stress or the strain tolerance because of the overriding influence of the multiaxiality introduced by the crack itself. Experimental verification of this assumption in linear elastic fracture mechanics is inconclusive.

\*\*This assumes that full thickness restraint exists in the 0.375 in. plate so that the strain tolerance is a minimum similar to plane strain fracture toughness. Experimental verification of this assumption is inconclusive.

by the applied strain ( $\lambda_a$ ) which is  $0.62/0.29$  or  $2.14$ . Since the safety factor against fracture is greater than the safety factor against yield, the vessel will malfunction first by general yielding of the membrane wall.

Let us now assume that inspection sensitivity is not quite as good as before, so that the maximum size flaw that might be missed is 15 percent of the wall thickness or 0.045 inches. For this case  $R/(R+a) = 0.96$ ,  $\lambda_c = 2.30\%$ ,  $\lambda_e = 1.79\%$ ,  $K_\lambda = 4.2$ , and  $\lambda_f = 0.43\%$ . The factor of safety is equal to  $0.43/0.29$  or  $1.48$ . In this case the vessel will malfunction first by fracturing at the nozzle opening.

ARTHUR LAKES LIBRARY  
COLORADO SCHOOL OF MINES  
GOLDEN, COLORADO

RECOMMENDATIONS FOR FUTURE WORK

There are a number of uncertainties still associated with design application of the strain tolerance fracture criteria that were indicated in the application-of-principle example presented in the previous section. Recommendations for future research are the following:

- (1) Effect of thickness restraint on strain tolerance.
- (2) Effect of stress state on strain tolerance.
- (3) Effect of flaw shape on strain tolerance.

APPENDIX A

STRAIN TOLERANCE DATA FOR 2014-T6 ALUMINUM  
(HEAT 6670), 6Al-4V TITANIUM-STA, AND A533B STEEL

Baseline center-crack strain tolerance data for 2014-T6 aluminum (heat 6670), 6Al-4V titanium, and A533B steel is given in Tables A-1, A-2, and A-3, respectively. The most accurate determination of strain tolerance was from strain gage measurements. Total strain at failure, or strain tolerance, was also estimated from a photogrid with 0.100-in. spacing, and from a tensile test. The strain tolerance estimates from the photogrid required addition of the measured plastic failure strain and the elastic strain as calculated from the failure stress. The strain tolerance estimates from the tensile curve reflect the total strain in the tensile test at the same stress level as caused failure in the flawed strain tolerance specimen. The photogrid strain tolerance is surprisingly close to that measured from the strain gages considering that the value is subject to averaging errors and optical precision. The strain values from the tensile curve are also in the same range as the strain gage measurements, though not as close as the photogrid values. On the basis of this limited data, it appears that strain tolerance could be estimated within 20 percent from one tensile test well instrumented with strain gages and several strain tolerance tests where only failure stress is measured.

TABLE A-1. Strain Tolerance Data for 2014-T6 Aluminum (Heat 6670)  
at Room Temperature

Specimen Number	Thickness t (in.)	Width W (in.)	Gross Area A <sub>g</sub> (in.)	Flaw Depth a (in.)	Flaw Length 2c (in.)	Depth Ratio a/t	Shape Ratio a/2c	Net Area A <sub>n</sub> (in. <sup>2</sup> )	Area Ratio A/A <sub>n</sub>
A6	0.375	3.502	1.313	-	-	-	-	1.313	1.000
A7	0.374	3.502	1.310	0.196	0.512	0.524	0.383	1.231	0.940
A8	0.376	3.501	1.316	0.157	0.403	0.418	0.390	1.266	0.962
A9	0.375	3.501	1.313	0.117	0.306	0.312	0.382	1.285	0.979
A10	0.376	3.501	1.316	0.054	0.126	0.144	0.429	1.311	0.996
A11	0.377	3.497	1.318	0.043	0.098	0.114	0.439	1.315	0.998
A12	0.375	3.503	1.314	0.030	0.070	0.080	0.429	1.312	0.998

ARTHUR LAKES LIBRARY  
COLORADO SCHOOL OF MINES  
GOLDEN, COLORADO

TABLE A-1 (Continued)

Specimen Number	Fracture Load (lb)	Final Net Area (in. <sup>2</sup> )	True Total Fracture Strain	True Fracture Stress (psi)	Stress Ratio
	$P_f$	$A_f$	$\lambda_f$ (in./in.)	$S_n$	$S_n/S_y$
			Photogrid	Area Reduction	
			Strain Gages	Tensile Curve	
A6 *	87,090	1.013	-	0.268	1.29
A7	73,920	-	0.0057	0.006	0.90
A8	81,070	-	0.0061	0.006	0.96
A9	83,590	-	0.0064	0.007	0.98
A10	88,280	-	0.0172	0.018	1.02
A11	89,460	-	0.0300	0.027	1.05
A12	90,660	-	0.046	0.043	1.08

True Yield Stress = 66,600 psi      Elastic Modulus =  $10.6 \times 10^6$  psi

True Ultimate Stress = 74,800 psi      Fracture Toughness =  $36.3 \text{ ksi} \sqrt{\text{in.}}$

True Ultimate Strain = 0.0733

\*Necked Before Failure - Fracture Strain Calculated from Area Reduction

- Stress Not Corrected for Triaxiality

TABLE A-2. Strain Tolerance Data for 6Al-4V Titanium-STA

at Room Temperature

Specimen Number	Thickness t (in.)	Width W (in.)	Gross Area A <sub>g</sub> (in. <sup>2</sup> )	Flaw Depth a (in.)	Flaw Length 2c (in.)	Depth Ratio a/t	Shape Ratio a/2c	Net Area A <sub>n</sub> (in. <sup>2</sup> )	Area Ratio A/A <sub>n</sub>
T2	0.085	1.999	0.1699	0.028	0.082	0.329	0.342	0.1681	0.989
T3	0.086	1.749	0.1504	-	-	-	-	0.1504	1.000
T4	0.086	1.747	0.1502	0.046	0.129	0.535	0.357	0.1456	0.969
T5	0.087	1.503	0.1308	0.024	0.047	0.276	0.511	0.1299	0.993
T6	0.086	1.496	0.1286	0.013	0.032	0.151	0.406	0.1283	0.998

TABLE A-2 (Continued)

Specimen Number	Fracture Load (lb)	Final Net Area (in. <sup>2</sup> )	$A_f$	Strain Gages	Photogrid	Tensile Curve	Area Reduction	True Fracture Stress (psi)	Stress Ratio
	$P_f$	$A_f$	$\lambda_f$ (in./in.)					$S_n$	$S/S_y$
T2	27,350	-	0.0150	-	0.014	-	-	163,600	1.02
T3*	21,690	0.0968	-	-	-	0.454	-	224,100	1.40
T4	21,100	-	0.0085	-	0.0087	-	-	144,900	0.90
T5	21,590	-	0.0179	0.017	0.021	-	-	167,500	1.04
T6*	21,480	0.1055	-	-	-	0.208	-	203,600	1.27

True Yield Stress = 160,300 psi      Elastic Modulus =  $17.0 \times 10^6$  psi

True Ultimate Stress = 172,900 psi      Fracture Toughness =  $47.0 \text{ ksi } \sqrt{\text{in.}}$

True Ultimate Strain = 0.0402

\*Necked Before Failure - Fracture Strain Calculated from Area Reduction

- Stress Not Corrected for Triaxiality

TABLE A-3. Strain Tolerance Data for A533B Steel at -20°F.

Specimen Number	Thickness $t$ (in.)	Width $W$ (in.)	Gross Area $A_g$ (in. <sup>2</sup> )	Flaw Depth $a$ (in.)	Flaw Length $2c$ (in.)	Depth Ratio $a/t$	Shape Ratio $a/2c$	Net Area $A_n$ (in. <sup>2</sup> )	Area Ratio $A_n/A_g$
S1	1.496	5.313	7.948	-	-	-	-	7.948	1.000
S2	1.495	5.302	7.926	0.228	0.482	0.153	0.473	7.840	0.989
S3	1.498	5.344	8.005	0.494	1.042	0.330	0.474	7.601	0.950

TABLE A-3. (Continued)

Specimen Number	Fracture Load $P_f$ (lb)	Final Net Area $A_f$ (in. <sup>2</sup> )	Strain Gages	Photogrid	Tensile Curve	Area Reduction	True Fracture Stress $S_n$ (psi)	Stress Ratio $S_n/S_y$
					$\lambda_f$ (in./in.)			
S1*	605,000	3.910	-	-	-	0.715	154,700	2.19
S2*	695,000	5.121	-	-	-	0.430	135,700	1.92
S3	535,000	-	-	-	0.00235	-	70,400	1.00

True Yield Stress = 70,600 psi  
 True Ultimate Stress = 105,300 psi  
 True Ultimate Strain = 0.116

Elastic Modulus =  $29.9 \times 10^6$  psi  
 Fracture Toughness = 66.0 ksi  $\sqrt{\text{in.}}$

\*Necked Before Failure - Fracture Strain Calculated from Area Reduction

-- Stress Not Corrected for Triaxiality

APPENDIX B

ELASTIC STRAIN TOLERANCE CALCULATIONS FROM  
LINEAR ELASTIC FRACTURE MECHANICS

The linear elastic stress intensity expression for a surface flaw is given<sup>(13)</sup> by

$$K_I = 1.1 \sqrt{\pi} S \sqrt{a/Q}, \quad (B-1)$$

where  $Q$  is the flaw shape parameter given by

$$Q = [\phi^2 - 0.212 (S/S_y)^2],$$

and  $\phi$  is the complete elliptic integral of the second kind given by

$$\phi = \int_0^{\pi/2} \sqrt{1 - \left(\frac{c^2 - a^2}{c^2}\right) \sin^2 \theta} \, d\theta.$$

At fracture,  $K_I$  becomes the fracture toughness,  $K_{Ic}$ ,  $S$  is the nominal failure stress,  $a$  is the crack depth,  $S_y$  is the yield strength, and  $c$  is the half-crack length. This expression will be used up to the yield strength since it contains the plastic zone size correction factor,  $0.212(S/S_y)^2$ .

Fracture toughness ( $K_{Ic}$ ) calculations for 2014-T6 aluminum (heat 6670) at 70°F, 6Al-4V titanium-STA at 70°F, and A533B steel at -20°F are given in Table B-1.

The strain tolerance versus flaw size curve in the elastic region can be determined by rewriting Equation (B-1) in terms of total fracture strain ( $\lambda_c$ ) using Hooke's Law as

$$\lambda_c = \left[ \frac{\sqrt{Q} K_{Ic}}{1.1 \sqrt{\pi} E} \right] / \sqrt{a}, \quad (B-2)$$

TABLE B-1. Fracture Toughness Data for 2014-T6 Aluminum, 6Al-4V Titanium-STA, and A533B Steel

Specimen Number	Thickness t (in.)	Width W (in.)	Gross Area A <sub>g</sub> (in. <sup>2</sup> )	Flaw Depth a (in.)	Flaw Length 2c (in.)	Depth Ratio a/t	Shape Ratio a/2c	Net Area A <sub>n</sub> (in. <sup>2</sup> )	Area Ratio A/A <sub>n</sub>
2014-T6 ALUMINUM (HEAT 6670)      Temp. = 70°F									
A7	0.374	3.502	1.310	0.196	0.512	0.524	0.383	1.231	0.940
A8	0.376	3.501	1.316	0.157	0.403	0.418	0.390	1.266	0.962
A9	0.375	3.501	1.313	0.117	0.306	0.312	0.382	1.285	0.979
6Al-4V TITANIUM - STA      Temp. = 70°F									
T4	0.086	1.747	0.1502	0.046	0.129	0.535	0.357	0.1456	0.969
A533B STEEL      Temp. = -20°F									
S3	1.498	5.344	8.005	0.494	1.042	0.330	0.474	7.601	0.950

TABLE B-1. (Continued)

Specimen Number	Fracture Load $P_f$	Fracture Stress $S_n$	Fracture Stress Ratio $S_n/S_y$	Flaw Shape Parameter $Q$	Fracture Toughness $K_{Ic}$
	(lb)	(psi)			$ksi\sqrt{in.}$
2014-T6 ALUMINUM (HEAT 6670) Temp. = 70°F					
A7	73,920	60,000	0.901	1.78	38.8
A8	81,070	64,000	0.961	1.77	37.2
A9	83,590	65,100	0.977	1.74	32.9
6Al-4V TITANIUM - STA Temp. = 70°F					
T4	21,100	144,900	0.906	1.66	47.0
A533B STEEL Temp. = -20°F					
S3	535,000	70,400	0.997	2.14	66.0

2014-T6 Aluminum (Heat 6670) Yield Strength = 66.6 ksi

6Al-4V Titanium-STA Yield Strength = 160.3 ksi

A533B Steel Yield Strength = 70.8 ksi

ARTHUR LAKES LIBRARY  
 COLORADO SCHOOL OF MINES  
 GOLDEN, COLORADO

where  $E$  is the elastic modulus. For 2014-T6 aluminum (66.6 ksi yield), using a flaw shape ratio ( $a/2c$ ) equal to 0.40, an average value of flaw shape parameter ( $Q$ ) equal to 1.88 over the range of  $0.5 \leq (S/S_y) \leq 1$ , an elastic modulus equal to  $10.6 \times 10^6$  psi, and a fracture toughness ( $K_{Ic}$ ) equal to 36.3 ksi  $\sqrt{\text{in.}}$ , the linear elastic strain tolerance versus flaw size expression is  $\lambda_c = 2.408 \times 10^{-3}/\sqrt{a}$ . For 6Al-4V titanium-STA (160.3 ksi yield), using ( $a/2c$ ) = 0.40,  $Q = 1.88$ ,  $E = 17.0 \times 10^6$  psi, and  $K_{Ic} = 47.0$  ksi  $\sqrt{\text{in.}}$ , the elastic strain tolerance versus flaw size expression is  $\lambda_c = 1.944 \times 10^{-3}/\sqrt{a}$ . For A533B steel at  $-20^\circ\text{F}$  (70.8 ksi yield), using ( $a/2c$ ) = 0.47,  $Q = 2.19$ ,  $E = 29.9 \times 10^6$  psi, and  $K_{Ic} = 66.0$  ksi  $\sqrt{\text{in.}}$ , the elastic strain tolerance versus flaw size expression is  $\lambda_c = 1.675 \times 10^{-3}/\sqrt{a}$ .

APPENDIX C

CALCULATION OF A SEMIEMPIRICAL EQUATION FOR  
STRAIN TOLERANCE IN THE ELASTIC-PLASTIC REGION

ARTHUR LAKES LIBRARY  
 COLORADO SCHOOL OF MINES  
 GOLDEN, COLORADO

A semiempirical equation, that describes the strain tolerance versus flaw size curve in the elastic-plastic region, can be developed by modifying the elastic strain tolerance expression calculated in Appendix B. The rapid increase in strain tolerance in the plastic region can be taken into account by use of a plastic strain multiplying factor such as  $(1+n\epsilon_c)$ , where  $\epsilon_c$  is the plastic part of the strain tolerance and  $n$  is an empirical constant. Rewriting Equation (B-2) in these terms, we have

$$\lambda_c = \left[ \frac{\sqrt{Q} K_{Ic}}{1.1\sqrt{\pi} E} \cdot \frac{1}{\sqrt{a}} \right] (1+n\epsilon_c). \quad (C-1)$$

The relationship between total strain ( $\lambda$ ) and plastic strain ( $\epsilon$ ) can be determined from a tensile test, where the stress versus plastic strain curve can be expressed as a power function of the form

$$S = B\epsilon^m, \quad \text{for } \epsilon > 0, \quad (C-2)$$

where  $m$  is the strain hardening exponent and  $B$  is the stress constant at unit strain. Rewriting Equation (C-2) in terms of elastic strain ( $e$ ) and plastic strain ( $\epsilon$ ), we have

$$e = S/E = B\epsilon^m/E, \quad \text{for } \epsilon > 0, \quad (C-3)$$

where  $E$  is the elastic modulus. Since total strain ( $\lambda$ ) is the sum of its elastic and plastic parts, we have

$$\lambda = e + \epsilon = B\epsilon^m/E + \epsilon, \quad \text{for } \epsilon > 0. \quad (C-4)$$

Equations (C-1) and (C-4) are sufficient to describe the complete strain tolerance versus flaw size curve up to the point of plastic necking instability. The empirical constants B and m are determined from tensile data, and the constant n is determined from strain tolerance data in the plastic region.

True stress versus true plastic strain curves (Equation (C-2)) for 2014-T6 aluminum (heat 6670), 6Al-4V titanium-STA, and A533B steel are given in Figures C-1, C-2, and C-3, respectively. Note that the curve for A533B steel at  $-20^{\circ}\text{F}$  assumes that the strain hardening exponent is the same as at  $70^{\circ}\text{F}$ . Also, note that it is necessary to use two equations to describe the A533B flow curve as it exhibits a discontinuous yield point. The relationship between total strain ( $\lambda$ ) and plastic strain ( $\epsilon$ ) can be calculated by substituting appropriate values of B, m, and elastic modulus (E) into Equation (C-4). The resulting equations are:

For 2014-T6 aluminum (heat 6670) --

$$\lambda = 7.755 \times 10^{-3} \epsilon^{.038} + \epsilon, \quad \text{for } \epsilon > 0$$

For 6Al-4V titanium-STA --

$$\lambda = 11.412 \times 10^{-3} \epsilon^{.030} + \epsilon, \quad \text{for } \epsilon > 0$$

For A533B steel ( $-20^{\circ}\text{F}$ ) --

$$\lambda = 2.370 \times 10^{-3} + \epsilon, \quad \text{for } 0 < \epsilon < 0.009$$

$$\lambda = 5.027 \times 10^{-3} \epsilon^{.160} + \epsilon, \quad \text{for } \epsilon \geq 0.009.$$

0 - 2014 - T6 Aluminum (Heat 6670)

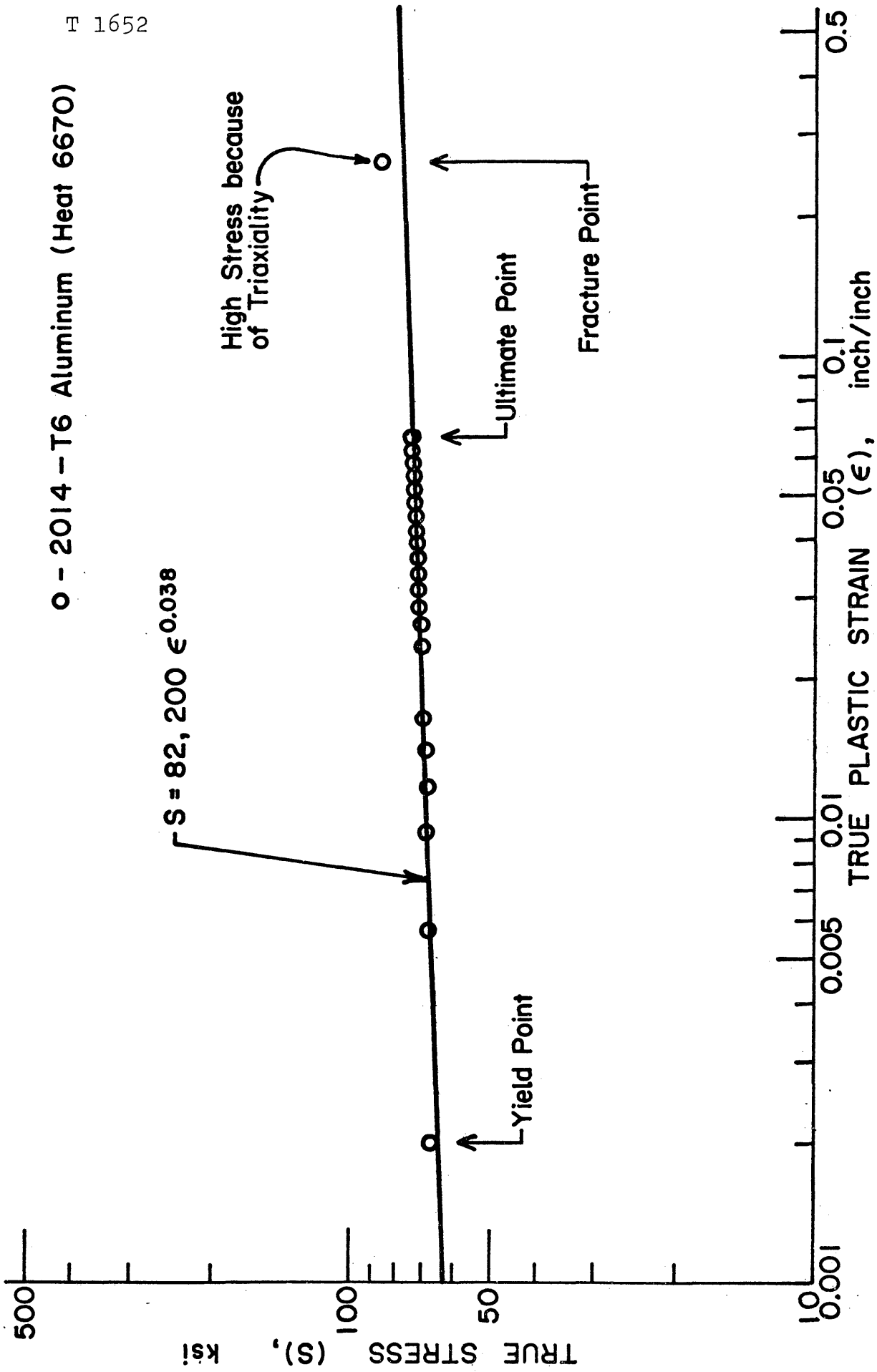


Figure C-1. Stress-Strain Curve for 2014-T6 Aluminum.

0 - 6Al-4V Titanium - STA

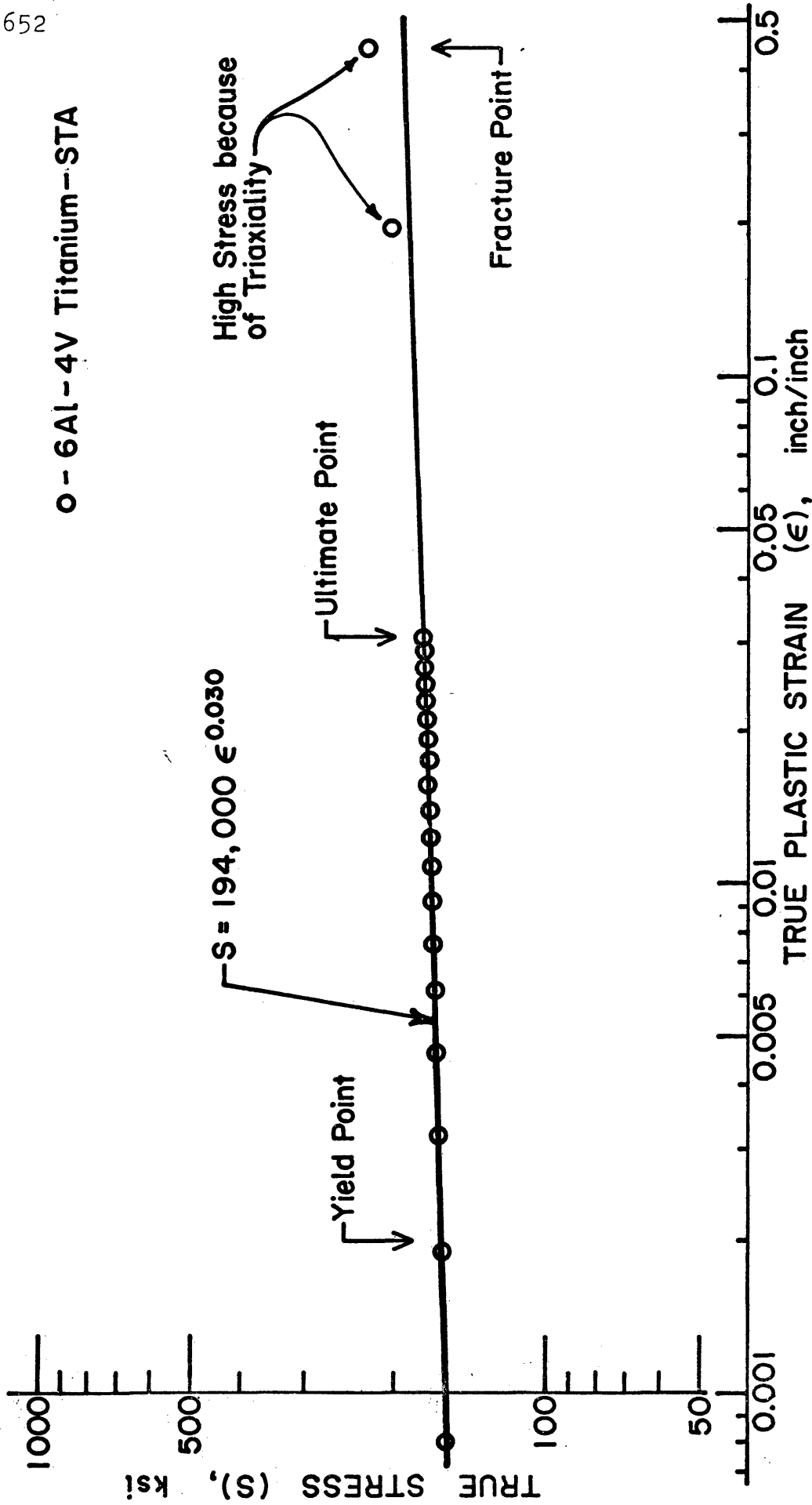


Figure C-2. Stress-Strain Curve for 6Al-4V Titanium-STA.

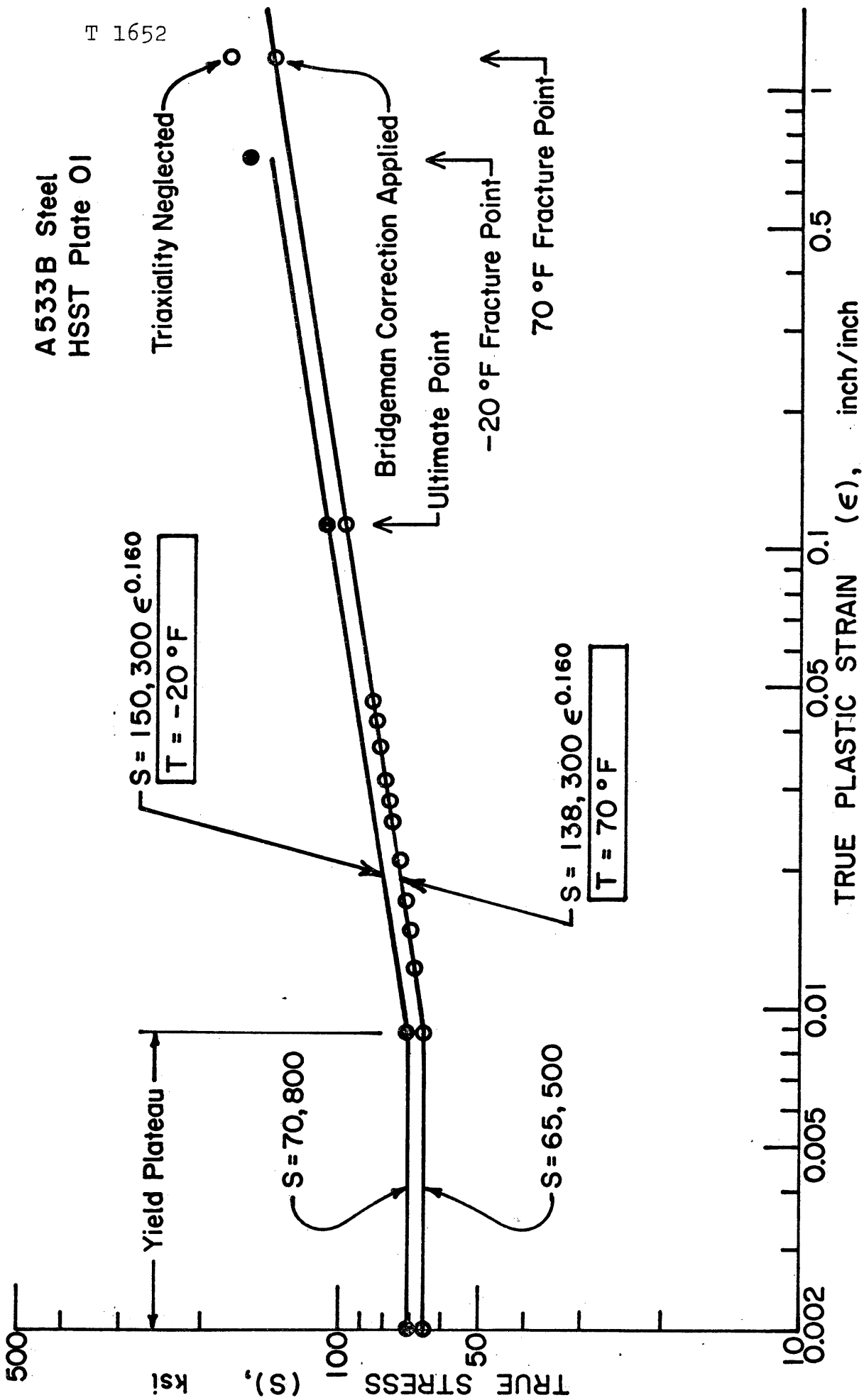


Figure C-3. Stress-Strain Curve for A533B Steel.

The empirical constant  $n$  in the strain tolerance versus crack size expression (Equation (C-1)) is determined by a best-fit of the experimental data points given in Appendix A. Appropriate values of the elastic parameters ( $Q$ ,  $K_{Ic}$ , and  $E$ ), strain tolerance ( $\lambda_c$ ), flaw depth ( $a$ ), and plastic strain ( $\epsilon_c$ ) are substituted into Equation (C-1) which is then solved for  $n$ . The resulting best-fit equations are:

For 2014-T6 aluminum (heat 6670) --

$$\lambda_c = \frac{2.408 \times 10^{-3}}{\sqrt{a}} (1 + 62 \epsilon_c)$$

For 6Al-4V titanium-STA --

$$\lambda_c = \frac{1.944 \times 10^{-3}}{\sqrt{a}} (1 + 56 \epsilon_c)$$

For A533B steel (-20°F) --

$$\lambda_c = \frac{1.675 \times 10^{-3}}{\sqrt{a}} (1 + 290 \epsilon_c).$$

APPENDIX D

NEUBER APPROXIMATION OF THE PLASTIC STRAIN  
CONCENTRATION FACTOR FOR A NOTCH

An analytical approximation of the plastic strain concentration factor for a notch under monotonic shear loading was developed by Neuber<sup>(20)</sup>. The basis of the Neuber approach is the suggested rule that the geometric mean of the plastic stress concentration factor ( $K_s$ ) and the plastic strain concentration factor ( $K_\lambda$ ) is equal to the theoretical elastic stress concentration factor ( $K_t$ ), or

$$(K_s K_\lambda)^{1/2} = K_t. \quad (D-1)$$

This relationship is derived from non-linear elastic theory for sharp notches and must be regarded as being purely empirical for non-linear elastic-plastic behavior. Equation (D-1) has been applied by Krempl<sup>(21)</sup> and Papirno<sup>(22)</sup> to tension and compression loading, where  $K_s$  is defined as the ratio of peak normal stress-to-net section normal stress ( $S_p/S_n$ ) and  $K_\lambda$  is defined as the ratio of peak normal strain-to-net section normal strain ( $\lambda_p/\lambda_n$ ).

For the completely elastic case where the stress-strain behavior, both in the net section and at the notch, can be expressed by Hooke's Law, Equation (D-1) reduces to

$$K_\lambda = K_t, \quad \text{for } \lambda_n \leq \frac{1}{K_t} (S_y/E), \quad (D-2)$$

where  $S_y$  is the yield strength and  $E$  is the elastic modulus.

For the case of an elastic net section and a plastic notch, two separate stress-strain equations are necessary to describe the material behavior at the two locations. For a

material with a plastic flow curve that can be expressed in the form of a power function, the stress-strain relation at the plastic notch is given by

$$S_p = B\lambda_p^m, \quad (D-3)$$

where  $m$  is the strain hardening exponent and  $B$  is the stress constant at unit strain. The stress-strain relation in the elastic net section is

$$S_n = E\lambda_n. \quad (D-4)$$

By substituting Equations (D-3) and (D-4) into Equation (D-1), the plastic strain concentration factor ( $K_\lambda$ ) can be expressed as

$$K_\lambda = K_t^{\frac{2\lambda}{1+m}} (E/B)^{\frac{1}{1+m}} \lambda_n^{\frac{1-m}{1+m}},$$

$$\text{for } (1/K_t)(S_y/E) \leq \lambda_n \leq S_y/E. \quad (D-5)$$

In this case, the plastic strain concentration factor ( $K_\lambda$ ) for a given notch ( $K_t$ ), is a function of elastic modulus ( $E$ ), material flow properties ( $B$ ,  $m$ ), and net section strain level ( $\lambda_n$ ).

For the fully plastic case, the stress-strain relation at the plastic notch is expressed, as before, by Equation (D-3). The stress-strain relation in the plastic net section is given by

$$S_n = B\lambda_n^m. \quad (D-6)$$

By substituting Equations (D-3) and (D-6) into Equation (D-1),

the plastic strain concentration factor ( $K_\lambda$ ) can be expressed as

$$K_\lambda = K_t^{\frac{2}{1+m}}, \quad \text{for } \lambda_n \geq S_y/E. \quad (D-7)$$

In this case, the plastic strain concentration factor ( $K_\lambda$ ), for a given notch ( $K_t$ ), is only dependent on the strain hardening exponent ( $m$ ).

For a circular hole ( $K_t = 3.0$ ) in 2014-T6 aluminum ( $E = 10.6 \times 10^6$  psi,  $S_y = 66,500$  psi,  $S = 85,000 \lambda^{.053*}$ ), the plastic strain concentration factor ( $K_\lambda$ ), from Equations (D-2), (D-5), and (D-7), is given by

$$\begin{aligned} K_\lambda &= 3.0, & \text{for } \lambda_n \leq 0.0021, \\ \text{and } K_\lambda &= 780\lambda_n^{.90}, & \text{for } 0.0021 \leq \lambda_n \leq 0.0063, \\ \text{and } K_\lambda &= 8.0, & \text{for } \lambda_n \geq 0.0063. \end{aligned}$$

---

\*This equation expresses the same flow behavior as the tensile curve in Appendix C, Figure (C-1), except that total strain ( $\lambda$ ) is used instead of plastic strain ( $\epsilon$ ).

APPENDIX E

ELASTIC STRAIN GRADIENT EFFECT FOR A CIRCULAR HOLE-EDGE  
CRACK GEOMETRY FROM LINEAR ELASTIC FRACTURE MECHANICS

Bowie<sup>(23)</sup> has applied Griffith's theory of brittle fracture to the case on an infinite plate containing two radial, diametrically opposite, through-thickness cracks of length  $a$  originating at the edge of an internal through-thickness hole of radius  $R$ . The circular hole-edge crack geometry is illustrated in Figure E-1. The plate is loaded in uniaxial tension perpendicular to the plane of the cracks, and is thick enough to provide full restraint. The length between the crack extremities is  $2(R+a)$  and the relative crack length is  $a/R$ .

In the limiting case where  $R$  equals zero and the infinite plate contains a single through-crack of length  $2a$  in a uniform stress field, the nominal fracture stress ( $S_u$ ) is expressed by

$$S_u = \frac{K_{Ic}}{(\pi a)^{1/2}}, \quad (E-1)$$

where  $K_{Ic}$  is the plane strain fracture toughness. Equation (E-1) can be rewritten in terms of nominal fracture strain (or strain tolerance),  $e_u$ , using Hooke's Law as

$$e_u = \frac{K_{Ic}}{E(\pi a)^{1/2}}, \quad (E-2)$$

where  $E$  is the elastic modulus.

In the general case where  $R$  is greater than zero and the cracks are influenced by the presence of the hole, Bowie expressed the nominal fracture stress ( $S_g$ ) as

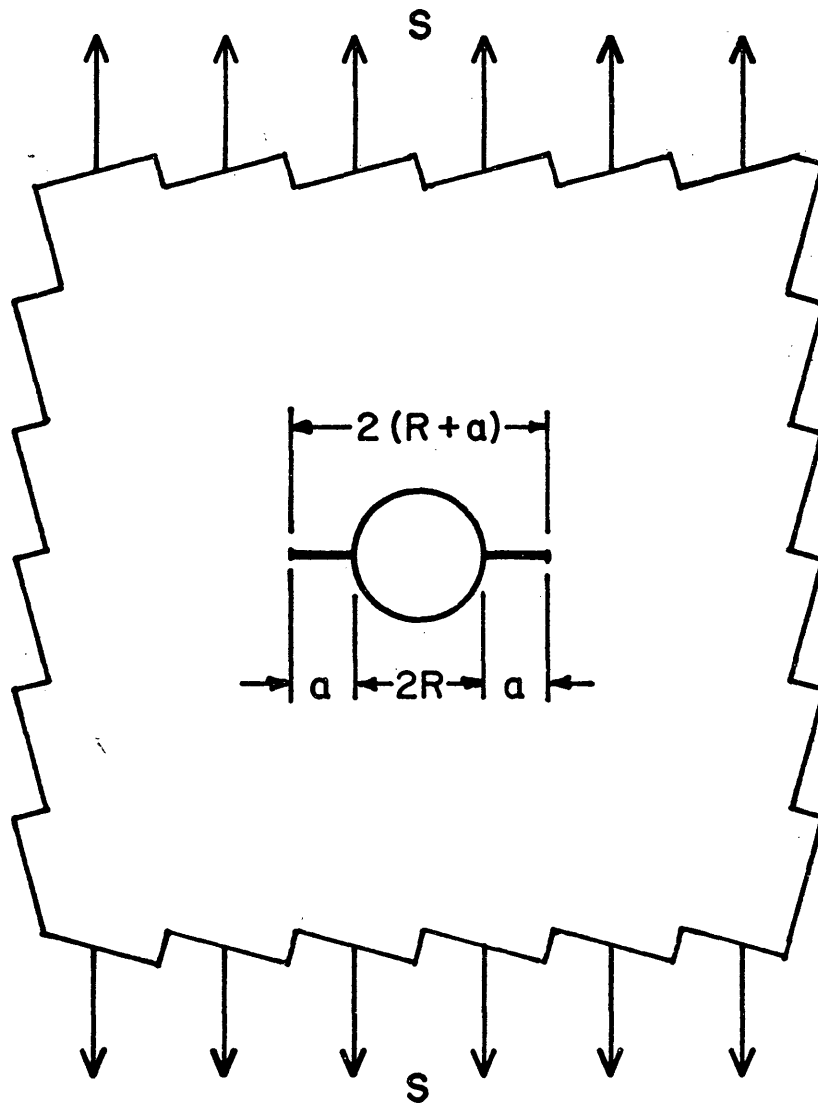


Figure E-1. Circular Hole-Edge Crack Geometry in Infinite Plate.

$$S_g = \left[ \frac{E G_c / 1 - \nu^2}{\pi R} \right]^{1/2} F(a/R), \quad (E-3)$$

where  $G_c$  is the critical strain energy release rate,  $\nu$  is Poisson's ratio, and  $F(a/R)$  is a stress function that takes account of the influence of the stress concentration gradient.  $F(a/R)$  is plotted in Figure E-2 as a function of relative crack length  $a/R$ . Equation (E-3) can be expressed in the more convenient form of equation (E-1) as

$$S_g = \frac{K_{Ic}}{(\pi a)^{1/2}} (a/R)^{1/2} F(a/R). \quad (E-4)$$

Equation (E-4) can be rewritten in terms of nominal fracture strain ( $e_g$ ) using Hooke's law as

$$e_g = \frac{K_{Ic}}{E(\pi a)^{1/2}} (a/R)^{1/2} F(a/R). \quad (E-5)$$

The effective strain tolerance is equal to the ratio of nominal fracture strain in the strain gradient-to-nominal fracture strain in a uniform strain field ( $e_g/e_u$ ). Dividing equation (E-2) by equation (E-5), we have

$$\frac{e_g}{e_u} = (a/R)^{1/2} F(a/R). \quad (E-6)$$

In order to express the whole range from zero hole size to infinite hole size, it is convenient to express strain gradient as the ratio,  $R/(R+a)$ , which will have values between 0 and 1. Effective strain tolerance is plotted as a function of strain gradient ratio in Figure E-3. For  $R/(R+a)$  equal

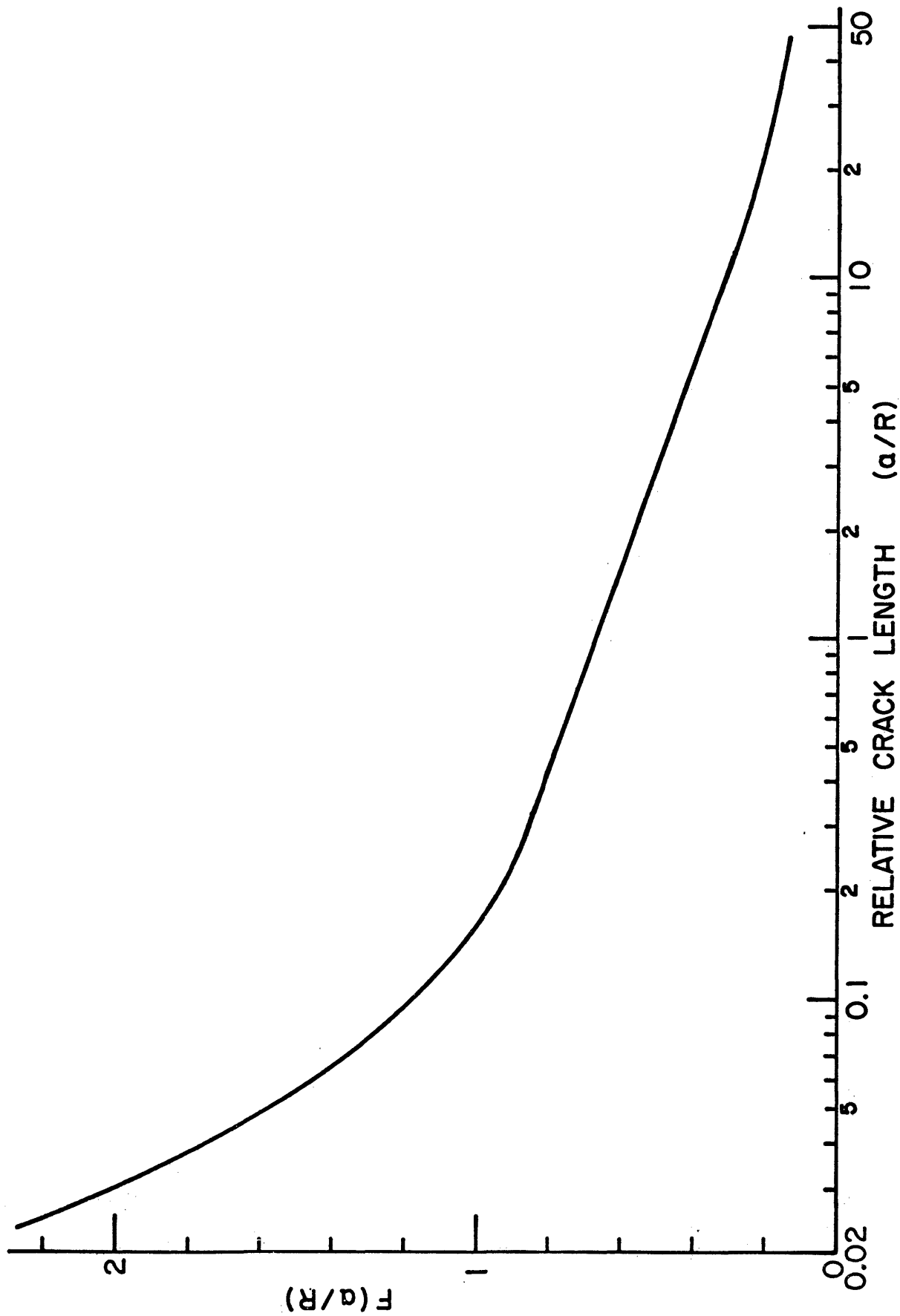


Figure E-2. Stress Function  $F(a/R)$  for Circular Hole-Edge Crack Geometry.

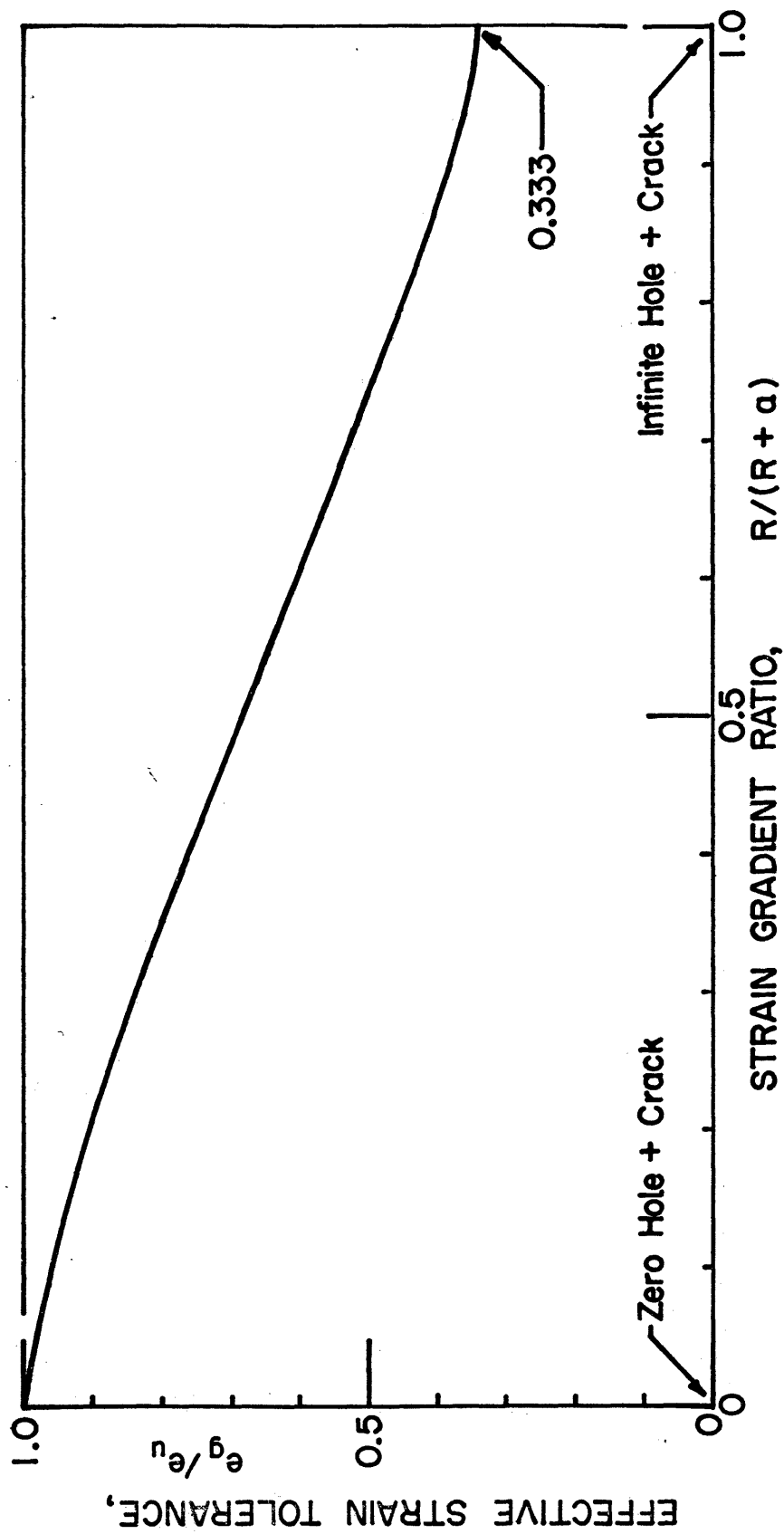


Figure E-3. Elastic Strain Gradient Effect for a Circular Hole-Edge Crack Geometry.

to zero, the effective strain tolerance is equal to 1, since the crack is in a uniform strain field. As  $R/(R+a)$  increases above zero, the effective strain tolerance decreases, even though the strain gradient is still too steep to affect the crack tip, because the crack length is effectively increased by the hole diameter. As  $R/(R+a)$  increases still further (decreasing strain gradient for a larger hole), the effective strain tolerance continues to decrease because of the more severe conditions that exist when the crack tip is subjected to a progressively higher strain in the strain gradient. As  $R/(R+a)$  approaches unity, the effective strain tolerance approaches a limiting value of 0.333\* for a crack that is subjected to the full strain concentration at an infinite hole. The fact that the nominal fracture strain for a crack that is subjected to the full strain concentration is  $1/3$  of the nominal fracture strain in a uniform strain field is not surprising, since the theoretical elastic strain concentration factor for a hole is 3. It is probable that effective strain tolerance in the elastic-plastic region will have a limiting value that is the reciprocal of the plastic strain concentration factor ( $K_\lambda$ ).

---

\*If this limiting value were to be checked experimentally, using a center-cracked sample for baseline strain tolerance in a uniform strain field, it would be 0.297. The reason for this discrepancy is that two edge-cracks of length  $a$  are 11 percent more severe than a center-crack of length  $2a$ . This geometry effect is not predicted by elasticity theory. If the baseline strain tolerance sample were an edge-cracked sample, the limiting value would be 0.333 as predicted.

It was implied in the foregoing discussion that there might be a limited region where the strain gradient due to a very small hole is so steep that the crack is essentially still in a region of uniform strain, except that the effective half-crack length ( $a_e$ ) is longer by the hole radius ( $R$ ). For this to be true, by inspection of Equations (E-2) and (E-5), the following identity must exist, namely that

$$\frac{1}{(a_e)^{1/2}} = \frac{1}{(a+R)^{1/2}} \approx \frac{1}{a^{1/2}} (a/R)^{1/2} F(a/R). \quad (\text{E-7})$$

Reducing Equation (E-7) to a simpler form, we have

$$1 + a/R \approx \left[ \frac{1}{F(a/R)} \right]^2. \quad (\text{E-8})$$

If  $1 + a/R$  is greater than  $[1/F(a/R)]^2$ , then  $a+R$  overestimates the effective crack length. If  $1 + a/R$  is less than  $[1/F(a/R)]^2$ , then  $a+R$  underestimates the effective crack length. For  $0 \leq R/(R+a) \leq 0.85$ ,  $1 + a/R$  is never different from  $[1/F(a/R)]^2$  by more than 3 percent on the average. Thus, for  $0 \leq R/(R+a) \leq 0.85$ , the effective half-crack length ( $a+R$ ) controls fracture behavior, and for  $0.85 < R/(R+a) \leq 1$ , the local strain field controls failure. Quarter-elliptical surface cracks at the edges of a hole may be affected by the local strain field out to values of  $R/(R+a)$  less than 0.85 since one point on the crack front will always be at the edge of the hole.

The effective strain tolerance curve in the elastic-plastic region might possibly be approximated by assuming

that the effective strain tolerance  $(EST)_\lambda$  should decrease between 1 and  $1/K_\lambda$  at the same rate as the elastic effective strain tolerance  $(EST)_e$  decreases between 1 and  $1/3$ . This can be expressed by the following two equations,

$$(EST)_e = 1/3 + P(1-1/3), \quad (E-9)$$

$$\text{and } (EST)_\lambda = 1/K_\lambda + P(1-1/K_\lambda), \quad (E-10)$$

where P is the proportioning constant. If equation (E-9) is rewritten as

$$P = \frac{3(EST)_e - 1}{2}, \quad (E-11)$$

and substituted into equation (E-10), we have

$$(EST)_\lambda = \frac{3}{2K_\lambda} [1 - (EST)_e] + 1/2 [3(EST)_e - 1], \quad (E-12)$$

which is an approximation curve for the elastic-plastic strain tolerance  $(EST)_\lambda$  as a function of plastic strain concentration factor ( $K_\lambda$ ) and the elastic effective strain tolerance curve  $(EST)_e$  in Figure E-3.

LITERATURE CITED

1. Williams, M. L., Analysis of Brittle Behavior in Ship Plates: Symposium on Effect of Temperature on the Brittle Behavior of Metals with Particular Reference to Low Temperatures, ASTM STP 158, p. 11-44 (1954).
2. Pellini, W. S., Evaluation of the Significance of Charpy Tests: Symposium on Effect of Temperature on the Brittle Behavior of Metals with Particular Reference to Low Temperatures, ASTM STP 158, p. 216-261 (1954).
3. Tiffany, C. F. and Masters, J. N., Applied Fracture Mechanics: Fracture Toughness Testing and Its Applications, ASTM STP 381, p. 249-277 (1965).
4. Hutchinson, J. W., Singular Behavior of the End of a Tensile Crack in Hardening Material: Journal of the Mechanics and Physics of Solids, Vol. 16, p. 13-31 (1968).
5. Rice, J. R. and Rosengren, G. F., Plane Strain Deformation Near a Crack Tip in a Power-Law Hardening Material: Journal of the Mechanics and Physics of Solids, Vol. 16, p. 1-12 (1968).
6. Hilton, P. D. and Hutchinson, J. W., Plastic Stress Intensity Factors for Cracked Plates: Harvard University Report SM-34 (1969).
7. Levy, N. and Marcal, P. V., Three-Dimensional Elastic-Plastic Stress and Strain Analysis for Fracture Mechanics: Brown University HSST Technical Report No. 12 (1970).
8. Rice, J. R., A Path Independent Integral and the Approximate Analysis of Strain Concentration by Notches and Cracks: Trans. ASME, Journal of Applied Mechanics, Vol. 90, p. 379-386 (1968).
9. Randall, P. N., Brittle Fracture Design Concepts--Fracture Mechanics Approach: ASME and ASTM Session on Factors Affecting Design and Performance of Pressure Vessels, Houston, Texas (1967).
10. Begley, J. A. and Landes, J. D., The J-Integral as a Fracture Criterion: Fracture Toughness, Proceedings of the 1971 National Symposium on Fracture Mechanics, Part II, ASTM STP 514, p. 1-20 (1972).

11. Landes, J. D. and Begley, J. A., The Effect of Specimen Geometry on  $J_{Ic}$ : Fracture Toughness, Proceedings of the 1971 National Symposium on Fracture Mechanics, Part II, ASTM STP 514, p. 24-39 (1972).
12. Lubahn, J. D., Design Criteria for Heavy Section Structures: in Fracture, Proceedings of the Second Tewksbury Symposium, University of Melbourne, p. 101-118 (1969).
13. Irwin, G. R., Crack Extension Force for a Part-Through Crack in a Plate: Trans. ASME, Journal of Applied Mechanics, Vol. 84, p. 651-654 (1962).
14. Fracture Design Guide, Prepared by ASME Research Committee on Prevention of Fracture in Metals (1971).
15. Brown, Jr., W. F. and Srawley, J. E., Plane Strain Crack Toughness Testing of High Strength Metallic Materials: ASTM STP 410 (1969).
16. Beck, E. J., Plastic Strain Distribution Measurements Around a Semielliptical Surface Flaw: M.Sc. Thesis T-1269, Colorado School of Mines (1969).
17. Beck, E. J., Personal communication (1971).
18. Loechel, L. W., The Effect of Testing Variables on the Transition Temperature in Steel: Report No. HSSTP-TR-2, Martin Marietta Aerospace (1969).
19. Peterson, R. E., Stress Concentration Design Factors, John Wiley & Sons, New York (1953).
20. Neuber, H., Theory of Stress Concentration for Shear Strained Prismatical Bodies with Arbitrary Nonlinear Stress-Strain Law: Trans. ASME, Journal of Applied Mechanics, Vol. 83, p. 544-550 (1961).
21. Krempl, E., Low-Cycle Fatigue Strength Reduction in Notched Flat Plates: ASME, Preprint 67-MET-13.
22. Papirno, R., Plastic Concentration Factors in Flat Notched Specimens of AISI 4340 Steel: Army Materials and Mechanics Research Center Report No. TR-70-2 (1970).
23. Bowie, O. L., Analysis of an Infinite Plate Containing Radial Cracks Originating at the Boundary of an Internal Circular Hole: Journal of Mathematics and Physics, Vol. 35, p. 60-71 (1956).

24. Derby, R. W., Shape Factors for Nozzle Corner Cracks: Experimental Mechanics, Vol. 12, No. 12, p. 580-584 (1972).